Spatially-distributed influence of agro-environmental factors governing nitrate fate and transport in an irrigated stream-aquifer system

Ryan T. Bailey[1], Mehdi Ahmadi[2], Timothy K. Gates[1], and Mazdak Arabi[1]

[1] {Department of Civil and Environmental Engineering, Colorado State University, 1372 Campus Delivery, Fort Collins, CO, 80523-1372, United States}

[2] {Department of Civil Engineering, Sharif University of Technology, Azadi St., Tehran, 11365-11155, Iran}

Correspondence to: R. T. Bailey (rtbailey@engr.colostate.edu)

Tel: 970-491-5045

Fax: 970-491-7727

20 **Abstract**

21 Elevated levels of nitrate (NO_3) in groundwater systems pose a serious risk to human populations

22 and natural ecosystems. As part of an effort to remediate NO_3 contamination in irrigated stream-

23 aquifer systems, this study elucidates agricultural and environmental parameters and processes

24 that govern NO_3 fate and transport at the regional (500 km^2), local (50 km^2), and field scales (< 1

25 km^2). Specifically, the revised Morris sensitivity analysis method was applied to a finite-

26 difference nitrogen cycling and reactive transport model of a regional-scale study site in the

27 Lower Arkansas River Valley in southeastern Colorado. The method was used to rank the

28 influence of anthropogenic activities and natural chemical processes on NO_3 groundwater

29 concentration, NO_3 mass leaching, and NO_3 mass loading to the Arkansas River from the

30 aquifer. Sensitivity indices were computed for the entire study area in aggregate as well as each

31 canal command area, crop type, and individual grid cells. Results suggest that fertilizer loading,

32 crop uptake, and heterotrophic denitrification govern NO_3 fate and transport for the majority of

33 the study area, although their order of influence on NO_3 groundwater concentration and mass

34 leaching varies according to crop type and command area. Canal NO_3 concentration and rates of

35 autotrophic denitrification, nitrification, and humus decomposition also dominate or partially

36 dominate in other locations. Each factor, with the exception of O_2 reduction rate, is the

37 dominating influence on NO_3 groundwater concentration at one or more locations within the

38 study area. Results can be used to determine critical processes and key management actions for

39 future data collection and remediation strategies, with efforts able to be focused on localized

40 areas.

41

42 **1 Introduction**

43 During recent decades, elevated concentration of nitrate (NO_3) C_{NO_3} in groundwater systems and

44 at points of groundwater discharge to surface water bodies has become a serious environmental

45 issue due to its adverse effects on human populations and natural ecosystems [Spalding and

46 Exner, 1993]. Specific problems associated with high C_{NO_3} include methemoglobinemia for

47 infants [Fan and Steinberg, 1996] and eutrophication in aquatic systems, which induces depletion

48   of dissolved oxygen (O_2) (hypoxia) due to increased biological activity. In addition, high C_{NO_3} can

49   lead to elevated concentrations of sulfate and selenium (Se) via oxidation of pyrite (FeS_2) and

50   seleno-pyrite ($FeSe_2$) from marine shale [Frind et al., 1990; Jørgensen et al., 2009; Bailey et al.,

51   2012]. NO₃ also has been shown to mobilize uranium via oxidation [Wu et al., 2010]. Recent

52   studies have revealed that certain rock formations can yield nitrogen (N) in response to a variety

53   of biogeochemical processes [Holloway and Dahlgren 2002, Montross et al 2013]. In most cases,

54   however, elevated concentrations result from excessive loadings of organic or inorganic N

55   fertilizer, inducing NO₃ leaching to the saturated zone of the aquifer [Korom, 1992; Spalding and

56   Exner, 1993].

57   To combat NO₃ contamination, numerous field and modeling studies have been performed to

58   quantify NO₃ fate and transport processes in soil-groundwater systems, identify baseline

59   conditions of N sources and transport patterns, and investigate potential remediation strategies.

60   For the latter, simulation models typically are used to predict the effect of land use and best-

61   managements practices (BMPs) such as reduction in fertilizer loading [Chaplot et al., 2004;

62   Almasri and Kaluarachchi, 2007; Lee et al., 2010], reduction in applied irrigation water [Ma et

63   al.,1998; Rong and Xuefeng, 2011], and implementing or enhancing riparian buffer zones

64   [Hefting and Klein, 1998; Spruill, 2000; Vaché et al., 2002; Sahu and Gu, 2009] on overall C_{NO_3}

65   and on NO₃ mass loading to and within streams. These studies have been conducted at various

66   scales [Ocampo et al., 2006], ranging from the soil profile and field scale [Johnsson et al., 1987;

67   Ma et al., 1998; Rong and Xuefeng, 2011], to the catchment scale [Birkinshaw and Ewen, 2000;

68   Conan et al., 2003; Wriedt and Rode, 2006; Lee et al., 2010], to the regional-scale watershed or

69   river basin scale [Chaplot et al., 2004; Almasri and Kaluarachchi, 2007; Bailey et al., 2015], and

70   include a variety of fate and transport processes such as soil N cycling, leaching, groundwater

71   transport, and overland transport.

72   Besides assessing baseline conditions and predicting domain-scale effects on spatial

73   concentrations and loadings, numerical models also can be used in NO₃ remediation to determine

74   the system inputs, parameters, and processes (i.e., model factors) that govern these

75   concentrations and loadings. In general, identifying the most influential processes on resulting

76   C_{NO_3} and mass loading can assist in establishing optimal remediation strategies. Additional

77   benefits of the analysis include guiding effective field sampling strategies by focusing on

78   influential system variables or inputs; facilitating model calibration and testing by focusing on

79   the identified key factors [Sincock et al., 2003; Almasri and Kaluarachchi, 2007]; identifying

80   factors that require additional research to improve model performance [Hall et al., 2009]; and

81   detecting non-influential parameters or processes that possibly could be eliminated to simplify

82   the model [Saltelli et al., 2008].

83   An appealing approach to determine the influence of model factors is sensitivity analysis (SA),

84   which relates changes in model output variables (e.g., concentration, mass loading) to prescribed

85   changes in model factor input values (e.g., initial conditions, system stresses, system

86   parameters). For studies assessing NO_3 fate and transport in groundwater systems using

87   physically-based spatially-distributed groundwater models, sensitivity analysis typically is

88   performed in a simple fashion due to model complexity and computational cost. For example,

89   Almasri and Kaluarachchi [2007] increased values of selected parameters (e.g., denitrification

90   rate, longitudinal dispersivity, initial concentration, soil mineralization rate, soil nitrification rate,

91   fertilizer loading) by 50% to determine their influence on simulated C_{NO_3} in a watershed in

92   Washington state, USA; Ehteshami et al. [2013], using the LEACHN model, investigated the

93   influence of low and high values of rainfall and initial C_{NO_3} for two soil types on soil C_{NO_3}. In a

94   field study using the RISK-N model, Oyarzun et al. [2007] modified values of soil initial N, C_{NO_3}

95   in irrigation water, fertilizer, N crop uptake, crop evapotranspiration (ET), and soil properties by

96   50%, 70%, 100%, 125%, and 150% to investigate their influence on NO_3 vadose zone mass flux

97   and C_{NO_3} in the groundwater. Also, Hartmann et al. [2013] used SA to estimate the influence of

98   model parameters on the time lag between spring discharge and NO_3 at several karst aquifer sites

99   across Europe. Whereas global effects of the model factor on system-response variables can be

100   assessed, local and interaction effects cannot be quantified.

101   A more rigorous SA method is global sensitivity analysis (GSA), which searches the entire

102   parameter space to identify the importance of model parameters and interactions thereof. Such

103   methods include the Elementary Effects (EE) method [Morris, 1991; Cacuci, 2003], a screening

104   method that identifies the most important model factors and is well-suited for large models

105   [Campolongo and Braddock, 1999], and variance-based methods that quantitatively decompose

106 the variance of model output into fractions that are attributed to model factors [Saltelli et al.,

107 2008]. A number of hydrologic modeling studies have used GSA methods for assessing model

108 factor influence on overall watershed nutrient and sediment processes [White and Chaubey,

109 2005; Arabi et al., 2007; Sun et al., 2012, Ahmadi et al., 2014], flooding and hydraulic

110 characteristics [Hall et al., 2005; Hall et al., 2009], in-stream water quality [Cox and Whitehead,

111 2005; Deflandre et al., 2006; Liu and Zou, 2012; Bailey and Ahmadi, 2014], and in-stream solute

112 transport [Kelleher et al., 2013].

113 Sensitivity analysis is commonly used in hydrologic and water quality modeling to identify the

114 influence of model parameters on an aggregated measure of model responses such as average

115 annual stream discharge or contaminant loads. A few studies have assessed how the results of SA

116 vary in time. For example Reusser et al. [2011] used hydrologic catchment models to investigate

117 the temporal-varying influence of model factors on a variety of watershed response variables for

118 catchments in Ecuador and Germany. However, the spatial variability of sensitivity indices has

119 been largely neglected. Specifically regarding this study, no studies have quantified the spatial-

120 varying influence of factors on solute concentrations in large-scale groundwater systems. Such

121 information could be valuable in terms of implementing site-specific remediation strategies,

122 facilitating model calibration for specific model domain regions, and identifying system

123 variables that require additional field data collection, particularly for NO_3 due to its ubiquitous

124 presence in groundwater systems worldwide.

125 This study aims to identify the spatially-varying influence of system factors on NO_3 fate and

126 transport in a regional-scale (506 km^2) irrigated hydro-agricultural system. Specifically, the

127 factors' influence on NO_3 groundwater concentrations, NO_3 leaching below root zone, and NO_3

128 groundwater mass loading to the stream network will be quantified for a variety of scales

129 (cultivated field, canal command area, region). A calibrated and tested N fate and transport

130 groundwater model is used for the assessment, with the modified Morris method used for the

131 sensitivity analysis.

132

133

2 Methods

A comprehensive SA method was applied to a regional-scale, intensively irrigated 506 km^2 groundwater system in the Lower Arkansas River Valley (LARV) in southeastern Colorado to identify the spatially-varying influence of system factors on NO_3 concentrations in groundwater, NO_3 mass leaching in the shallow soil zone, and NO_3 mass loading to the Arkansas River. The model used is UZF-RT3D [Bailey et al., 2013a, 2013b], a MODFLOW [Niswonger et al., 2011] based, finite-difference model designed for N fate and transport at the regional scale and recently calibrated and tested for the study area [Bailey et al., 2014]. The model accounts for major agricultural inputs (fertilizer, canal seepage, irrigation water), processes (N cycling in the root and soil zone, leaching, three-dimensional transport, heterotrophic and autotrophic denitrification), and outputs (mass loading to the stream network).

As identifying the relative importance of parameters and processes in space is the objective of this study, and since computational costs of UZF-RT3D are extremely high (run-time of approximately 3.5 hours for a single simulation using an Intel® Core™ i7-3770 CPU @ 3.40GHz desktop computer), the SA method used is an improved variant [Campolongo et al., 2007] of the Morris method [Morris, 1991] rather than variance-based SA methods such as Sobol' [Sobol', 1993] or FAST (Fourier Amplitude Sensitivity Test) [Cukier et al., 1973]. Nine model factors are included in the assessment, with their overall influence on NO_3 fate and transport evidenced in a previous study in the region [Bailey et al., 2014]. In conjunction with the SA methodology, model results are processed to determine the dominant model factors globally (i.e., averaged for the entire model domain), for each irrigation canal command area, for each crop type (i.e., the set of model grid cells associated with each crop type), and for each grid cell, thereby elucidating parameter influence at varying spatial scales. For the latter, spatial contour maps depicting model sensitivity to individual model factors are shown. Due to the dependence of N fate and transport on the presence of O_2, the influence of the 9 model input factors on C_{O_2} also is calculated and presented.

162 **2.1 Study Area**

163 The semi-arid LARV in Colorado extends from the outlet of the Arkansas River from Pueblo

164 Reservoir eastward across southeastern Colorado to the border with Kansas (Figure 1), with the

165 Arkansas River fed primarily by snowmelt from the mountainous regions of the upper Arkansas

166 basin. In total, the valley supports approximately 109,000 irrigated ha (270,000 ac), and is one of

167 Colorado's most productive agricultural areas. Approximately 14,000 fields are cultivated, with

168 the majority using flood irrigation methods and a small minority using sprinklers or drip

169 irrigation methods. Major crops include alfalfa, corn, grass hay, wheat, sorghum, dry beans,

170 cantaloupe, watermelon, melons, and onions.

171 The region of the LARV focused on in this study is shown in Figure 1. The boundary of the

172 study area is shown with a black line, and encompasses an area of 50,600 ha (125,000 ac), of

173 which 26,400 ha (65,300 ac) are irrigated. The fields receiving water from each of six main

174 irrigation canals (i.e. canal command areas) are shown in Figure 2a, with crop type cultivated in

175 2006 for each field shown in Figure 2b. Due to over-irrigation and poor subsurface drainage,

176 high water table elevations have been established in recent decades, with water table depth below

177 ground surface often between 1-3 m [Morway and Gates, 2012]. These high water tables have

178 resulted in salinization and waterlogging, in addition to substantial rates of groundwater return

179 flows (i.e. discharge) to the Arkansas River and its tributaries [Morway et al., 2013]. The

180 thickness of the alluvial aquifer ranges from 4 to 34 m (Figure 4a), and is underlain by

181 Cretaceous Shale [Scott, 1968; Sharps, 1976] in both solid and weathered form.

182 In addition to salinization and associated decrease in crop productivity [Morway and Gates,

183 2012], elevated groundwater C_{NO_3} has been observed, presumably due to over-fertilization on

184 cultivated fields. In a similar irrigated region of the LARV, located about 67 km upstream,

185 Zielinski et al. [1997] examined $\delta^{15}N$ isotopic signatures to conclude that NO₃ was derived

186 primarily from fertilizer and crop waste, not from proximate geologic sources. To assess the

187 C_{NO_3} in the study region, groundwater and surface water samples were collected (see locations in

188 Figure 2a) during 10 sampling events over the period 2006-2009 [Gates et al. 2009]. For

189 groundwater, samples were taken routinely from 52 observation wells, with groundwater from 37

190   additional observation wells sampled non-routinely (aperiodic). Surface water samples were

191   taken from 10 locations along the Arkansas River and 5 locations in tributaries. Detailed results

192   of the monitoring scheme are shown in Supplementary Data. In summary, for groundwater the

193   85th percentile values of C_{NO_3-N} were at or in excess of the 10 mg/L (85th percentile) EPA

194   drinking water standard for the first three sample trips. The maximum measured value was 66

195   mg/L. The means for the samples gathered from the Arkansas River and its tributaries were 1.53

196   mg/L and 1.95 mg/L, respectively. The annual median values of the Arkansas River samples

197   were 0.95, 1.20, 1.10, and 2.20 mg/L for each of the successive years within the period 2006 -

198   2009, compared to the Colorado interim standard of 2 mg/L [CDPHE, 2012] for total inorganic

199   N concentration ($C_{NO_3-N} + C_{NO_2-N} + C_{NH_4-N}$). The concentration of C_{NO_3-N} exceeded 2 mg/L in

200   about 25% of the samples gathered in the river over this period and exceeded 2.5 mg/L in about

201   12% of the samples, signifying the growing concern about N pollution in the river. Analysis of

202   22 river samples and 15 tributary samples in 2013 revealed that C_{NO_3-N} made up greater than 80%

203   of total dissolved N in the river and about 76% of total dissolved N in the tributaries.

2.2 UZF-RT3D N Reaction Module and Baseline Application

205   UZF-RT3D simulates the reactive transport of multiple interacting chemical species in variably-

206   saturated porous media using groundwater flow rates, water content, and a variety of

207   groundwater sources and sinks (e.g., applied irrigation water, pumping, canal seepage,

208   groundwater-surface water interactions) simulated by a MODFLOW-NWT model using the

209   UZF1 package. The N cycling and reaction module add-on package [Bailey et al., 2013b] was

210   designed for model application in an irrigated agricultural groundwater system, and accounts for

211   the major hydrologic, chemical, and land management processes that govern N fate and transport

212   in an irrigated stream-aquifer system. Also, due to the dependence of N cycling and transport on

213   the presence of O_2, the fate and transport of O_2 is included.

214   A schematic of the fate and transport of N species and O_2 as simulated by the N reaction module

215   of UZF-RT3D is depicted in Figure 3a. N mass (NO_3 or NH_4) enters the subsurface via fertilizer

216   loading (single application or split application), canal seepage, infiltrating irrigation water (either

217   from canal water or pumped groundwater), or seepage from the stream network (Arkansas River

218   and its tributaries). N mass exits the subsurface via groundwater discharge to the stream network.

219   N cycling occurs in the root and soil zone, with organic N and carbon (C) added to soil organic

220   matter (manure M_N, fast-decomposing litter L_N, flow-decomposing humus H_N) via after-harvest

221   plowing or decaying root mass and subsequently mineralized to NH_4, which can be volatilized,

222   nitrified to NO_3, or taken up with NO_3 into crop roots during the growing season. The timing of

223   land management actions, e.g. fertilizer loading (40%, 60% split application), irrigation events,

224   harvesting, and plowing, adopted in the module is shown in Figure 3b. NH_4 is sorbed readily to

225   soil surface sites, whereas NO_3 is transported by one-dimensional transport in the unsaturated

226   zone and three-dimensional transport in the saturated zone, subject to heterotrophic

227   denitrification in near-surface areas and autotrophic denitrification in the presence of FeS_2-

228   bearing marine shale (see Figure 1). O_2 also is subject to heterotrophic and autotrophic chemical

229   reduction.

230   UZF-RT3D solves a system of advection-dispersion-reaction (ADR) equations for interacting

231   dissolved-phase and solid-phase species using the finite-difference approach. Including ADR

232   processes and source/sink terms as depicted, the following mass conservation equations are

233   written for the dissolved-phase species (NO_3, NH_4, O_2) in the N reaction module:

$$\frac{\partial\left(C_{NH_4}\theta\right)}{\partial t}R_{NH_4} = -\frac{\partial}{\partial x_i}\left(\theta v_i C_{NH_4}\right)+\frac{\partial}{\partial x_i}\left(\theta D_{ij}\frac{\partial C_{NH_4}}{\partial x_j}\right)+q_f C_{f_{NH_4}}+F_{NH_4}-U_{NH_4}+\varepsilon\left(r_{s,N}^{min}-r_{s,N}^{imm}\right)$$
$$+\ \theta\left(-r_f^{nit}-r_f^{vol}\right)$$
$$(1)$$

$$\frac{\partial\left(C_{NO_3}\theta\right)}{\partial t} = -\frac{\partial}{\partial x_i}\left(\theta v_i C_{NO_3}\right)+\frac{\partial}{\partial x_i}\left(\theta D_{ij}\frac{\partial C_{NO_3}}{\partial x_j}\right)+q_f C_{f_{NO_3}}+F_{NO_3}-U_{NO_3}+\ \theta\left(r_f^{nit}-r_{f,NO_3}^{het}-r_{f,NO_3}^{auto}\right)$$
$$(2)$$

$$\frac{\partial\left(C_{O_2}\theta\right)}{\partial t} = -\frac{\partial}{\partial x_i}\left(\theta v_i C_{O_2}\right)+\frac{\partial}{\partial x_i}\left(\theta D_{ij}\frac{\partial C_{O_2}}{\partial x_j}\right)+q_f C_{f_{O_2}}+\theta\left(-r_{f,O_2}^{het}-r_{f,O_2}^{auto}\right)$$
$$(3)$$

234   where C is solute concentration [$M_f L_f^{-3}$], with f denoting fluid phase; v is the pore velocity [L_bT⁻

235   ¹], provided by MODFLOW-UZF1; θ is the volumetric water content [$L_f^3 L_b^{-3}$], also provided by

236   MODFLOW-UZF1; D_{ij} is the hydrodynamic dispersion coefficient [$L^2 T^{-1}$]; q_f is the volumetric

237   flux of water representing sources and sinks $[L_f^3 T^{-1} L_b^{-3}]$ such as irrigation water, canal and river

238   seepage, groundwater discharge to the river, or pumped groundwater, with b denoting the bulk

239   phase; C_f is the concentration of the source or sink $[M_f L_f^{-3}]$; F is the inorganic fertilizer

240   application $[M_f L_b^{-3} T^{-1}]$; U is the potential crop uptake rate $[M_f L_b^{-3} T^{-1}]$; ε is the volumetric solid

241   content $[L_s^3 L_b^{-3}]$ with s denoting the solid phase, and is equal to $1-\phi$, where ϕ is porosity $[L_f^3 L_b^{-}$

242     $^3]$; r_f represents the rate of all reactions that occur in the dissolved-phase $[M_f L_f^{-3} T^{-1}]$; *min, imm,*

243   *nit*, and *vol* signify mineralization, immobilization, nitrification, and volatilization of NH_4,

244   respectively; and *auto* and *het* represent autotrophic and heterotrophic chemical reduction,

245   respectively. ε is included for the min and imm reactions to denote a mass transfer between the

246   solid and dissolved phases. For NH_4, which is subject to sorption, R is the retardation factor and

247   is equal to $1 + (\rho_b K_{d,NH_4})/\theta$, where ρ_b is the bulk density of the porous media $[M_b L_b^{-3}]$ and

248   K_{d,NH_4} is the partitioning coefficient $[L_f^{-3} M_b]$. The daily mass of potential N crop uptake during

249   the growing season is determined using a logistic equation [Johnsson et al., 1987] and is

250   distributed across the vertical column of grid cells encompassing the crop rooting depth

251   according to the mass density of the root system. Mass conservation equations (not shown) for

252   solid-phase organic N (and C) species L_N, H_N, and M_N also are implemented.

253   The rate of chemical reactions r_f included in Equations (1-3) is governed by the dependence of

254   the chemical reaction on soil temperature T, θ, and the presence of O_2 and C. These rates are

255   simulated using first-order Monod kinetics. For example, the following rate law expression

256   represents the process of heterotrophic denitrification, with others contained in Bailey et al.

257   [2015]:

$$r_{f,NO_3}^{het} = \lambda_{NO_3}^{het} C_{NO_3} \left(\frac{C_{NO_3}}{K_{NO_3} + C_{NO_3}} \right) \left(\frac{CO_{2,prod}}{K_{CO_2} + CO_{2,prod}} \right) \left(\frac{I_{O_2}}{I_{O_2} + C_{O_2}} \right) E \tag{4}$$

258   where λ is the base rate constant for the reaction $[T^{-1}]$; K_j is the Monod half-saturation constant

259   for species j $[M_f L_f^{-3}]$; I_{O_2} is the O_2 inhibition constant $[M_f L_f^{-3}]$ signifying the species concentration

260   at which lower-redox species can undergo appreciable rates of reduction; $CO_{2,prod}$ is the total

261   mass of CO_2 produced during organic matter decomposition and is used as an indicator of

262   available organic carbon (OC) for microbial consumption [Birkinshaw and Ewen, 2000]; and E

263   [-] is an environmental reduction factor that accounts for θ and T and acts to temper microbial

264   activity rates [Birkinshaw and Ewen, 2000; Bailey et al., 2013b]. Nitrification, mineralization,

265   and denitrification each have uniquely specified relationships between θ and microbial activity.

266   The UZF-RT3D model used in this study is the same as that described in Bailey et al. [2014].

267   The model uses output from a calibrated and tested MODFLOW-NWT [Niswonger et al., 2011]

268   model of the study region [Morway et al., 2013], which uses the UZF1 unsaturated-zone flow

269   package [Niswonger et al., 2006]. The flow model uses weekly estimates of irrigation water,

270   precipitation, canal seepage, crop ET to estimate groundwater level and groundwater-surface

271   water interactions for the 1999-2009 time period. Figures 4b, 4c, and 4d show the finite-

272   difference grid, the simulated water content of the soil in June 2006, and the average simulated

273   water table elevation (m) during the 1999-2009 time period, respectively.

274   The UZF-RT3D model uses the same model domain and finite difference grid as the flow model

275   (see Figure 4b). The model has 7 vertical layers, with Layers 1-2 (0.5 m each) corresponding to

276   the root zone, Layer 3 (1.0 m) corresponding to the leaching zone, Layers 4-6 to the saturated

277   zone, and Layer 7 to the shale bedrock formation. Thickness of layers 4, 5, and 6 varies

278   according to saturated thickness, with layer thickness ranging from 2.8 m to 12.6 m. Each

279   vertical column of cells in the 3D grid is assigned a set of crop parameter values according to the

280   portions of fields within the grid cell area. Crop parameters, with values shown in Table 1 for

281   each crop type in the study area, include: Planting Day; Harvest Day; Plowing Day; mass of

282   stover plowed into the soil P_{St} (kg/ha) after harvest; maximum rooting depth $d_{rt,max}$ (m), which

283   controls N uptake; C-N ratio of root mass CN_{RT}; fertilizer loading F_{NH_4} (kg/ha), maximum

284   seasonal uptake values of N N_{up} (kg/ha), depth of plowing d_{pw} (m); mass of decaying roots P_{Rt}

285   (kg/ha); C-N ratio of stover mass CN_{ST}; and constants defining root growth and daily uptake rate

286   U. Chemical reaction parameter values are shown in Table 2, with an asterisk * indicating the

287   mean value of all the grid cells. C_{NO_3} and C_{O_2} of canal water and irrigation water were based on

288   observed data. The model was run for the 2006-2009 and tested against spatio-temporal averages

289   of groundwater C_{NO_3} and NO₃ mass loadings from the aquifer to the Arkansas River.

2.3 Assessing Major Controls on NO₃ Fate and Transport

2.3.1 Morris SA Methodology

The Morris screening method for global SA is based on an individually randomized one-at-a-time (OAT) design that provides information regarding (i) the main effect of each input parameter on model output responses and (ii) the overall effects including interactions between parameters. For example, consider a model M with a vector of k parameters $(\omega_i, i = 1,...,k)$ within the feasible parameter space, $\mathbf{\Omega}$, that simulates m response vectors of the system $(S_j, j = 1,...,m)$:

$$[S_1,...,S_m] = M(\omega_1,...,\omega_k) \tag{5}$$

Similar to any standard SA practice, parameters are drawn from their predefined distributions, with each model input parameter ω_i varied across p discrete values [Saltelli et al., 2008]. Generally, results of SA are not sensitive to the choice of distribution from which values are sampled. After running model M for the given parameter sets, the local sensitivity measure (also referred to as the *elementary effect*, *EE*) is then computed for each parameter i for model response j as follows:

$$EE_{i,j}(\boldsymbol{\omega}) = \left(\frac{S_j(\omega_1,...,\omega_{i-1},\omega_i+\Delta,...\omega_k) - S_j(\boldsymbol{\omega})}{\Delta} \right) \tag{6}$$

where Δ is a value in the predefined increments (i.e. $\left[1/(p-1),...,1-1/(p-1) \right]$) and $\boldsymbol{\omega} = \omega_1,...,\omega_k$ is a random sample in the parameter space so that the transformed point $(\omega_1,...,\omega_{i-1},\omega_i+\Delta,...\omega_k)$ is still within the parameter space $\mathbf{\Omega}$ [Saltelli et al., 2008]. The resulting distribution EE_i associated with each parameter ω_i is then analyzed to determine μ, the mean of the distribution which assesses the overall importance of the parameter on the model output; and σ, the standard deviation of the distribution, which indicates non-linear effects and/or interactions [Campolongo et al., 2007].

310   To determine sensitive and insensitive values, it is recommended to evaluate a graphical

311   representation of σ vs. μ. However, for non-monotonic models, some *EE* values with opposite

312   signs may cancel out when μ is calculated, and hence Campolongo and Saltelli [1997] proposed

313   the use of μ^*, the sample mean of the distribution of absolute values of *EE*. μ^* includes all types

314   of effects that parameters can have on output responses and, therefore, is a global measure of

315   output sensitivity to the parameters [Campolongo et al., 2007]. $\mu^*_{i,j}$ is defined as the mean of

316   absolute values of the computed elementary effects $EE_{i,j}$. The total computational cost of the

317   Morris experiment is $n = r(k+1)$ runs, where r is the selected size of each sample.

318   As noted above, an important objective of SA is to determine the most influential model input

319   parameters. Hence, it is important to measure the level of agreement between results of SA

320   experiments with an emphasis on the high-ranked parameters. Campolongo and Saltelli [1997]

321   suggested the use of the Savage score to facilitate comparison of results from different SA

322   experiments (see next section). The Savage score is defined as follows [Iman and Conover,

323   1987]:

$$SS_i = \sum_{h=i}^{k} \frac{1}{h} \qquad (7)$$

324   where i is the rank assigned to the ith model parameter based on the Morris μ^*. For example, the

325   highest ranked variable would have a score of $1/1 + \frac{1}{2} + 1/3 + \ldots + 1/k$. The second ranked

326   variable would have a score of $\frac{1}{2} + 1/3 + \ldots + 1/k$, and so on. Savage scores typically are

327   preferred because they place higher emphasis on the agreement of the key drivers (i.e. higher

328   ranked parameters), rather than the overall agreement. The Savage score can be used in

329   aggregating the results from different SA methods.

330 2.3.2 Model Input Factors Analyzed

331   In applying the SA method to the UZF-RT3D model of the study area, 9 model input factors

332   were analyzed for impact on model results: F_{NH_4}, N_{up}, C_{NO_3} in canal water $Canal_{NO_3}$, rate of litter

333   pool decomposition λ_L, rate of humus pool decomposition λ_H, rate of autotrophic reduction of O_2

334   in the presence of shale $\lambda_{O_2}^{auto}$, rate of autotrophic reduction of NO_3 in the presence of shale $\lambda_{NO_3}^{auto}$,

335   rate of nitrification λ_{nit}, and rate of heterotrophic denitrification $\lambda_{NO_3}^{het}$. $Canal_{NO_3}$ conveys NO_3 mass

336   into the subsurface system via applied irrigation water as well as seeped canal water. For each

337   simulation, separate values of F_{NH_4} and N_{up} were generated for each crop type, separate values of

338    $Canal_{NO_3}$ were generated for each of the six canal command areas, and separate values of $\lambda_{O_2}^{auto}$,

339    $\lambda_{NO_3}^{auto}$, and λ_{nit} were generated for each command area. The mean of each parameter value is

340   derived from the baseline simulation (see Tables 1 and 2), with the mean values of $\lambda_{O_2}^{auto}$, $\lambda_{NO_3}^{auto}$,

341   and λ_{nit} for each command area estimated during the calibration phase [Bailey et al., 2014].

342   Setting the number of replications r and levels p of the Morris scheme to 20 and 10, respectively,

343   a total of 280 simulations were run. Parameter values were perturbed using a coefficient of

344   variation (CV) of 0.2 for all parameters except for $Canal_{NO_3}$, which was perturbed with a CV of

345   0.1 based on variance in observed canal water concentrations. Perturbation for the reaction rates

346   (λ_L, λ_H, $\lambda_{O_2}^{auto}$, $\lambda_{NO_3}^{auto}$, $\lambda_{NO_3}^{het}$, λ_{nit}) was performed using log values since statistically these rates

347   typically conform to a lognormal distribution [Parkin and Robinson, 1989; McNab and Dooher,

348   1998]. CV values were selected by comparing the resulting spread of parameter values to values

349   found in the literature and from field data in the study area. The values of F_{NH_4}, $\lambda_{NO_3}^{auto}$, and

350    $Canal_{NO_3}$ for each of the 280 simulations are shown in Figure 5, with averages of 250 kg/ha,

351   1.055×10^{-4} day^{-1}, and 2.6 g m^{-3}, respectively. The values shown in Figure 5a are for grid cells

352   that contain corn, and the values shown in Figures 5b and 5c are for the grid cells within the

353   Rocky Ford Highline canal command area (canal feeding the gray-shaded fields in Figure 2a).

354   For each of the 280 simulations, the model was run for a 2-year spin-up period, followed by the

355   2006-2009 period. Model results were processed to determine the influence of the 9 targeted

356   model input factors on groundwater C_{NO_3}, NO_3 mass leached from the root zone, and total NO_3

357   mass loading to the Arkansas River from the aquifer. Post-processing was implemented to

358   determine this influence (i) globally for the entire study area, i.e. averaging values from all grid

359   cells; (ii) for individual crop types, i.e. averaging values from all grid cells corresponding to a

360   given crop type; (iii) for individual canal command areas, i.e. averaging values from all grid cells

361   within a given command areas; and (iv) for individual grid cells. As total NO_3 mass loading to

362   the Arkansas River occurs along the entire reach of the river within the study area, parameter

363   influence is assessed only for (i). Values of average concentration, average leaching, and total

364   mass loading were processed from the final year of the model simulation (i.e. 2009). For

365   groundwater C_{NO_3}, concentration values were taken from Layer 4 of the model, which

366   corresponds to the depth of observation well screens in the study area. For NO_3 leaching, values

367   are taken from Layer 3 (i.e. the mass leached from Layer 3 to Layer 4). For parameter influence

368   on C_{NO_3} for individual grid cells (item iv), the Savage score as calculated by Equation (7) will be

369   used for presentation of results. Also for (iv), the parameter influence on C_{O_2} will be presented.

370

3 Results and Discussion

3.1 General Model Results

373   Model results from one of the 280 simulations is shown in Figure 6, with spatial distribution of

374   C_{O_2} and C_{NO_3} shown in Figures 6a and 6b, respectively for July 22, 2009, and the spatial

375   distribution of NO_3 mass loading shown for one week during the winter (December 2 2006,

376   Figure 6c) and one week during the summer (August 10 2008, Figure 6d). Mass loadings from

377   the aquifer to the stream network (discharge) are displayed in red, whereas loadings from the

378   stream network to the aquifer (seepage) are displayed in green. For concentrations in

379   groundwater, values of C_{O_2} range from 0.0 to 10.3 mg/L, with an average value of 2.7 g m^{-3} for

380   the 7,776 active grid cells. Values of C_{NO_3} range from 0.0 to 78.3 mg/L, with an average value of

381   1.84 mg/L.

382   Hotspots occur for both C_{O_2} and C_{NO_3}, with those of C_{NO_3} typically occurring in locations of corn

383   cultivation due to the higher loading of F_{NH_4} as compared to other crop types. NO_3 mass loadings

384   occur along the Arkansas River and the tributaries, with discharge and seepage both occurring

385   along the length of the canals during the summer (Figure 6d). The spatio-temporal average value

386   of C_{NO_3} in groundwater for each command area during the entire 2006-2009 time period is shown

387   in Figure 7 for each of the 280 simulations. The average value for all grid cells in non-cultivated

388   area also is shown. Average C_{NO_3} across all simulations for each command area are (average of

389   observed field values are in parentheses) Highline 2.0 mg/L (3.1 mg/L); Catlin: 1.4 mg/L (6.1

390   mg/L); Rocky Ford: 1.5 mg/L (3.8 mg/L); Fort Lyon: 3.7 mg/L (1.6 mg/L); Holbrook: 1.9 mg/L

391   (3.5 mg/L); and non-cultivated areas: 3.5 mg/L (4.2 mg/L). Average values correspond closely to

392   results from the tested baseline model [Bailey et al., 2014].

3.2 Parameter influence on global concentration, leaching, and loading of NO₃

393

394   The global influence of the 9 model input factors on NO₃ fate and transport in the study area is

395   shown in Figure 8. Global sensitivity plots are used, with non-linear effects and/or interactions σ

396   plotted against mean $\mu*$. The influence of the factors on C_{NO_3} in Layer 1 (top 0.5 m of the root

397   zone), C_{NO_3} in Layer 4 (shallow saturated zone), NO₃ leaching from Layers 3 to 4 $L_{NO_3 Lay3 \to 4}$

398   (generally from the unsaturated zone to the saturated zone), and total NO₃ mass loading to the

399   Arkansas River $Load_{NO_3}$ are shown in Figures 8a, 8b, 8c, and 8d, respectively. As seen in Figure

400   8a, C_{NO_3} in the root zone is governed principally by fertilizer loading (F_{NH_4}) and seasonal NO₃

401   uptake by crops (N_{up}) and to a smaller degree by heterotrophic denitrification ($\lambda_{NO_3}^{het}$) and

402   nitrification (λ_{nit}). In the shallow saturated zone (Figure 8b), where NO₃ mass is received from

403   the upper soil zone via leaching, F_{NH_4} and N_{up} still are dominant, but the concentration of NO₃ in

404   the canals ($Canal_{NO_3}$) has a stronger direct impact than $\lambda_{NO_3}^{het}$. The rate of humus decomposition (

405   λ_H) and autotrophic denitrification ($\lambda_{NO_3}^{auto}$) also have a slight impact. NO₃ leaching also is

406   governed by F_{NH_4}, N_{up}, $\lambda_{NO_3}^{het}$, $Canal_{NO_3}$, and λ_H (Figure 8c), as higher F_{NH_4}, lower N_{up}, lower $\lambda_{NO_3}^{het}$

407   , and higher $Canal_{NO_3}$ increase the mass of NO₃ leached, and vice versa. $Load_{NO_3}$ is governed by

408   F_{NH_4}, N_{up}, and $\lambda_{NO_3}^{het}$ (Figure 8d), with $\lambda_{NO_3}^{het}$ influencing not only how much NO₃ is leached to the

409   water table and carried to the stream network via groundwater flow, but also how much NO₃

410   undergoes denitrification in the riparian areas of the stream network.

411 The high σ values for N_{up}, F_{NH_4}, $\lambda_{NO_3}^{het}$ and $Canal_{NO_3}$ shown in Figure 8 signify the large spread in

412 *EE* values for these parameters, indicating that their influence on C_{NO_3}, NO₃ leaching, and NO₃

413 mass loading is strongly dependent on the values of other parameters. For example, in reference

414 to C_{NO_3} in the shallow saturated zone (Figure 8b), the value of μ^* for N_{up} signifies the average

415 effect of N_{up} on C_{NO_3}, but some values of *EE* for N_{up} are much smaller and larger than μ^*.

416 Smaller values of *EE* indicate that the combined influence of other parameter values produced a

417 small effect of crop uptake on C_{NO_3}, such as a lower N fertilizer loading and higher rates of

418 denitrification, whereas larger values indicate that other parameters produced a larger effect of

419 crop uptake on C_{NO_3}, such as a higher N fertilizer loading and lower rates of denitrification. Also,

420 higher values of $Canal_{NO_3}$ increase the influence of crop uptake on C_{NO_3}, as more NO₃ mass is

421 brought into the soil zone via canal seepage and infiltrating irrigation water.

422 **3.3 Parameter influence on C_{NO_3} and leaching for each crop type**

423 The influence of each of the 9 parameters on C_{NO_3} in the shallow groundwater zone and on NO₃

424 leaching for each crop type in the study area is summarized in Tables 3 and 4, respectively using

425 values of μ^*. The μ^* values of the 3 most influential parameters for each crop type are bolded.

426 For the majority of crop types, C_{NO_3} in the shallow groundwater zone is governed by N fertilizer

427 loading (F_{NH_4}), seasonal crop N uptake (N_{up}), and heterotrophic denitrification $\lambda_{NO_3}^{het}$ (Table 3),

428 similar to the global analysis of C_{NO_3} in the shallow soil layers as presented in Section 3.2. For

429 example, μ^* for F_{NH_4}, N_{up}, and $\lambda_{NO_3}^{het}$ is 0.94, 0.72, and 0.30, respectively, for corn-cultivated

430 areas, and 0.84, 0.81, and 0.28 for sorghum-cultivated areas. The exception is areas that cultivate

431 onion, in which $Canal_{NO_3}$ ($\mu^* = 0.45$) ranks in the top three behind F_{NH_4} (1.21) and N_{up} (0.99).This

432 is due to the fact that onions receive irrigation water (from the canals) more frequently than do

433 the other crop types. Hence, the C_{NO_3} of the canal water has a stronger influence on groundwater

434 C_{NO_3} underlying onion-cultivated fields than for the other crop types. For many of the crops, λ_H

435 and λ_{nit} have a small to moderate influence, whereas litter pool decomposition rate (λ_L),

436   autotrophic reduction of O_2 ($\lambda_{O_2}^{auto}$), and autotrophic denitrification ($\lambda_{NO_3}^{auto}$) have a negligible to

437   small influence on C_{NO_3}.

438   The influence of the 9 parameters on NO_3 mass leaching to the shallow saturated zone (Table 4)

439   follows the same pattern as for their influence on C_{NO_3}, with fertilizer N loading, uptake, and

440   denitrification dictating the amount of NO_3 leached to the water table (values in boxes) and canal

441   concentration, nitrification, and humus and litter pool decomposition having small to moderate

442   values of $\mu*$. For corn-cultivated areas, the average effect $\mu*$ of F_{NH_4}, N_{up}, and $\lambda_{NO_3}^{het}$ is 486.3,

443   366.8, and 172.3, respectively, compared to 51.3 for λ_H, 41.3 for $Canal_{NO_3}$, and 26.4 for λ_L, with

444   15.2, 1.0, and 0.2 for λ_{nit}, $\lambda_{NO_3}^{auto}$, and $\lambda_{O_2}^{auto}$, respectively. Again, $Canal_{NO_3}$ is the third most

445   influential parameter for onion-cultivated areas, with $\mu* = 1.6$, compared to 9.7 and 7.2 for F_{NH_4}

446   and N_{up}, respectively.

447   **3.4 Parameter influence on C_{NO_3} and leaching in individual canal command areas**

448   Summaries of the influence of each of the 9 parameters on C_{NO_3} in the shallow groundwater zone

449   and on NO_3 leaching for each canal command area also are provided in Tables 3 and 4. The

450   results show important differences between the command areas, with a mixture of F_{NH_4}, N_{up}, λ_{nit},

451     $\lambda_{NO_3}^{het}$, $\lambda_{NO_3}^{auto}$, and $Canal_{NO_3}$ providing noteworthy impacts on C_{NO_3} and NO_3 mass leaching. For

452   influence on C_{NO_3} (Table 3), the top three influential parameters within the Catlin command area

453   are N_{up} ($\mu* = 0.26$), λ_{nit} (0.16), and F_{NH_4} (0.12), whereas the top three for the Rocky Ford

454   command area are $Canal_{NO_3}$ (0.51), $\lambda_{NO_3}^{auto}$ (0.20), and N_{up} (0.15), with the strong influence of $\lambda_{NO_3}^{auto}$

455   due to the presence of outcropped shale in the command area and hence locations of autotrophic

456   denitrification. $\lambda_{NO_3}^{auto}$ also has a strong influence in the Holbrook command area, with the third

457   highest value of $\mu*$ (0.11). $Canal_{NO_3}$ is ranked 3rd or higher in terms of $\mu*$ in 3 of the 6 command

458   areas (Rocky Ford, Otero, Highline). F_{NH_4}, N_{up}, and $\lambda_{NO_3}^{het}$ govern NO_3 mass leaching for each of

459   the command areas (Table 4) except for the Catlin command area, in which λ_{nit} is ranked second

460   ($\mu^* = 38.0$) and the Rocky Ford Ditch, in which $Canal_{NO_3}$ is ranked first ($\mu^* = 30.3$).

3.5 Spatial distribution of parameter influence on C_{NO_3} and C_{O_2}

461

462   Cell-by-cell plots of Savage scores for the parameters according to their ranking in influencing

463   C_{NO_3} in shallow groundwater are shown in Figure 9. Plots are presented for each of the targeted 9

464   parameters except for $\lambda_{O_2}^{auto}$ due to the negligible influence of O_2 autotrophic reduction on C_{NO_3}.

465   The value for each cell represents the ranking (1-9) and associated Savage score for the given

466   parameter. High ranking is displayed in maroon-red coloring, whereas low ranking is displayed

467   in blue. As seen in the plots, the ranking of each parameter in its influence on groundwater C_{NO_3}

468   is highly spatially-variable. For example, the locations where canal NO₃ concentration ($Canal_{NO_3}$

469   ) has the strongest influence (maroon coloring) (Figure 9b) are scattered throughout the region,

470   with entire local areas (encompassed by circles in Figure 9b) governed by this parameter. For the

471   cultivated areas, the dominant intputs/processes are fertilizer loading (Figure 9a), crop N uptake

472   (Figure 9d), and heterotrophic denitrification ($\lambda_{NO_3}^{het}$) (Figure 9e), with humus decomposition

473   (Figure 9g) having a moderate influence and litter decomposition (Figure 9h) having a small

474   influence. Whereas fertilizer loading and N uptake have the most influence on C_{NO_3} in most of the

475   cultivated areas, some areas are governed principally by heterotrophic denitrification and humus

476   decomposition (cells colored in maroon in Figures 9e and 9g). Denitrification is particularly

477   important in riparian areas along tributaries and the Arkansas River (Figure 9e), where dense

478   vegetation provides a natural filter of NO₃ before being loaded to surface water. Values of humus

479   decomposition (λ_H) and litter decomposition (λ_L) control the rate of organic C and organic N

480   decomposition and hence the availability of C for heterotrophic denitrification to proceed.

481   No area has λ_L being the dominant influence on C_{NO_3}. Nitrification rate has a strong impact on

482   C_{NO_3} in the Holbrook command area (red-pink cell coloring in Figure 9c), with small impact

483   elsewhere in the study area. Autotrophic denitrification is the dominant parameter in areas along

484   the Arkansas River and several of the tributaries (Figure 9f) that are adjacent to shale formations

485   (see Figure 1). However, it is interesting to note that there are many locations in the study area

486   adjacent to outcropped shale in which $\lambda_{NO_3}^{auto}$ is not the dominant parameter. These locations are

487   indicated by circles in Figure 9f. In these areas, other system inputs and processes such as F_{NH_4},

488   N_{up}, $\lambda_{NO_3}^{het}$ and λ_H are the governing influences on C_{NO_3}, demonstrating that knowledge of shale

489   locations alone cannot be used to determine where C_{NO_3} will be affected the most by autotrophic

490   denitrification.

491   Similar cell-by-cell plots of parameter Savage scores are shown in Figure 10 for influence on

492   C_{O_2} in shallow groundwater. λ_H and λ_L govern C_{O_2} in the cultivated areas (Figures 10c,d), with

493   F_{NH_4} (Figure 10b), N_{up} (Figure 10e) and $Canal_{NO_3}$ (Figure 10a) exhibiting small to moderate

494   influence on C_{O_2} in the cultivated areas. The strong influence of λ_H and λ_L occurs due to their

495   control of the rate of organic C decomposition, and hence the availability of C for heterotrophic

496   reduction of O_2. The rate of autotrophic reduction of O_2 ($\lambda_{O_2}^{auto}$) is dominant in localized areas

497   where shale is present (see maroon-shaded cells in Figure 10f) with small influences in other

498   areas of the study region, mainly in areas down-gradient of the shale areas.

499

4 Discussion of Results

501   Results provide information regarding the system inputs and processes that control NO_3 fate and

502   transport generally (across the entire study region), by crop type, by canal command area, and by

503   local regions. For the entire study region, detailed field sampling and observation of N fertilizer

504   loading, N crop uptake, heterotrophic denitrification in the shallow soil layers, and concentration

505   of NO_3 in canal water must be performed as often as possible to provide accurate model input

506   data. NO_3 in canal water not only seeps through the perimeter of the earthen irrigation canals into

507   the aquifer, but also is loaded to cultivated fields via applied irrigation water. In addition, results

508   indicate these inputs and processes must be controlled via implemented management practices if

509   NO_3 groundwater concentration, NO_3 leaching, and NO_3 mass loading to the river network are

510 expected to decline in future decades, whereas other processes (organic N decomposition,

511 nitrification of NH_4) are not critical target factors.

512 These results agree with other previous studies from regions worldwide, which indicated that key

513 controls on NO_3 fate and transport in groundwater and watershed systems, and hence targets for

514 management action, include N fertilizer application [Chaplot et al., 2004; Botter et al., 2006;

515 Almasri and Kaluarachchi, 2007; Arabi et al., 2007; Bailey et al., 2015] and rate of

516 denitrification [Wriedt and Rode, 2006; Almasri and Kaluarachchi, 2007; Schilling et al., 2007],

517 with the order of their influence varied depending on the study region. However, these studies

518 did not analyze the influence of NO_3 in canal irrigation water or the influence of crop N uptake.

519 Molénat and Gascuel-Odoux [2002] did demonstrate the strong influence of NO_3 leaching on in-

520 stream NO_3 concentration, similar to our assessment of N uptake and denitrification (which

521 influence NO3 leaching) on NO_3 loading from the aquifer to the stream network.

522 The same system parameters that govern NO_3 fate and transport at the regional scale also govern

523 NO_3 for each individual crop type. N fertilizer loading (less), N crop uptake (more), and

524 heterotrophic denitrification (more) typically must be controlled to decrease groundwater NO_3

525 concentration and NO_3 leaching, with NO_3 concentration in canal water controlled to lower these

526 values for onion-cultivated areas. For canal command areas, N fertilizer loading and N uptake

527 must be managed to decrease groundwater NO_3 concentration and NO_3 mass leaching in the

528 majority of command areas. However, nitrification of NH_4 is an important control for the Catlin

529 command area, NO_3 concentration in canal water is important for the Highline, Otero, and Rocky

530 Ford command areas, heterotrophic denitrification is important for each command area except

531 Catlin and Rocky Ford Ditch, and autotrophic denitrification is important for only the Holbrook

532 and Rocky Ford Ditch command areas. These reaction rate parameters must be focused on in

533 field data monitoring scheme and in model parameter estimation. Results demonstrate that

534 targeted inputs/outputs and processes vary depending on command area.

535 Similarly, different targets are required for controlling NO_3 fate and transport in localized areas

536 throughout the study region. In reference to Figure 9, each system parameter, with the exception

537 of litter pool decomposition, is the most influential in controlling NO_3 fate and transport in at

538 least several areas within the study region. N fertilizer loading is the dominant parameter in the

539   majority of cultivated areas, although N uptake, heterotrophic denitrification, and NO₃

540   concentration in canal water also are the most influential in much of the study area. The rate of

541   autotrophic denitrification ($\lambda_{NO_3}^{auto}$) is influential in many of the areas adjacent to outcropped

542   marine shale. However, it is interesting to note that there are many locations in the study area

543   adjacent to outcropped shale in which $\lambda_{NO_3}^{auto}$ is not the dominant parameter. These locations are

544   indicated by circles in Figure 9f. In these areas, other system inputs and processes are dominant,

545   demonstrating that knowledge of shale locations alone cannot be used to determine where

546   groundwater NO₃ concentration will be affected the most by autotrophic denitrification.

547   Whereas other studies [Chaplot et al., 2004; Botter et al., 2006; Wriedt and Rode, 2006; Almasri

548   and Kaluarachchi, 2007; Arabi et al., 2007; Schilling et al., 2007; Bailey et al., 2015] have

549   focused on the response of the entire groundwater and/or watershed system, the novelty of this

550   study is the assessment of NO₃ transport control in localized areas within a region. Almasri and

551   Kaluarachchi [2007] stated that the importance of denitrification in controlling NO₃ in

552   groundwater may differ from location to location. In this study we quantify this difference

553   spatially for denitrification and for each of the other eight targeted parameters (see Figure 9).

554

555   **5 Summary and Concluding Remarks**

556   This study used a 506 km^2 regional-scale N fate and transport numerical model to examine the

557   influence of forcing terms (fertilizer loading, crop N uptake, N concentration of applied

558   irrigation water and canal seepage $Canal_{NO_3}$) and chemical processes (litter and humus organic N

559   decomposition; nitrification of NH₄ to NO₃; heterotrophic and autotrophic reduction of NO₃,

560   with the latter occurring in the presence of pyrite-bearing marine shale; and autotrophic

561   reduction of O₂, also occurring in the presence of shale) on NO₃ concentration in groundwater

562   C_{NO_3}, NO₃ leaching from the unsaturated zone to the saturated zone of the aquifer, and NO₃ mass

563   loading from the aquifer to the Arkansas River via groundwater discharge. The influence of each

564   of the 9 model factors was computed using the revised Morris method for sensitivity analysis,

565   with results processed to determine parameter influence globally for the entire study region and

566   specific to crop type, canal command area (i.e. the group of fields receiving irrigation water from

567   a given canal), and individual grid cells. For the latter, spatial plots of sensitivity indices are

568   presented to display the spatial distribution of influence for each model factor.

569   Results indicate that, generally, fertilizer loading, crop N uptake, and heterotrophic

570   denitrification governed NO_3 mass transport, particularly in cultivated areas. However, their

571   order of influence on C_{NO_3} and NO_3 mass leaching varies according to crop type and command

572   area, and several command areas are influenced more, or at least to a significant degree, by

573   nitrification, autotrophic denitrification, and $Canal_{NO_3}$. Spatial plots of cell-by-cell sensitivity

574   indices enhance further the understanding of localized model factor influence, with each factor

575   except for rate of heterotrophic O_2 reduction having the dominant influence over C_{NO_3} at one or

576   more locations within the study area. Results also indicate that the concentration of O_2 in

577   groundwater C_{O_2} is governed by rates of organic matter decomposition, which releases CO_2 and

578   hence enhances heterotrophic reduction of O_2.

579   In general, the procedure followed in this study provides key information regarding overall NO_3

580   fate and transport in an agricultural groundwater system, guidance for future data collection and

581   monitoring programs, an indication of which parameters should be targeted during model

582   parameter estimation, and guidance for implementing best-management practices (BMPs) for

583   NO_3 remediation, i.e. decreasing groundwater concentrations and mass loading to the stream

584   network. For example, fertilizer loading, crop N uptake, and $Canal_{NO_3}$ should be targeted in field

585   data collection and observation, with $Canal_{NO_3}$ monitored for each irrigation canal as often as

586   possible, whereas first-order kinetic rate constants for nitrification, denitrification, and organic

587   matter decomposition should be targeted during parameter estimation efforts. Furthermore, the

588   procedure followed in this study also allows for data collection, management practice

589   implementation, and parameter estimation to be performed on location-specific basis. For

590   example, results suggest that a specific BMP (e.g., reduction in N fertilizer loading) may be

591   optimal for several of the command areas but not for others, or that decreasing $Canal_{NO_3}$ or the

592   amount of NO_3 denitrified in shale outcrop locations will help remediate NO_3 only in a few

593   specific locations within the study area. Also, data collecting points for specific model factors

594 can be restricted to sub-region areas, either to a given command area or, with the use of the

595 spatial plots of sensitivity indices, to even more localized sites.

596

597

610

611

612 **References**

613 Almasri, M.N., and J.J. Kaluarachchi (2007), Modeling nitrate contamination of groundwater in

614 agricultural watersheds. J. Hydrol. 343: 211-229.

615 Arabi, M., R.S. Govindaraju, B. Engel, and M. Hantush (2007), Multiobjective sensitivity

616 analysis of sediment and nitrogen processes with a watershed model. Water Resources Research

617 43, W06409,doi:10.1029/2006WR005463.

618 Bailey, R.T., W.J. Hunter, and T.K. Gates (2012), The influence of nitrate on selenium in

619 irrigated agricultural groundwater systems. J. Environ. Qual. 41(3): 783-792.

620   Bailey, R.T., E.D. Morway, R. Niswonger, and T.K. Gates (2013a), Modeling variably saturated
621   multispecies reactive groundwater solute transport with MODFLOW-UZF and RT3D.
622   Groundwater 51(5): 752-761.

623   Bailey, R.T., T.K. Gates, and A.D. Halvorson (2013b), Simulating variably-saturated reactive
624   transport of selenium and nitrogen in agricultural groundwater systems. J. Contam. Hydrol. 149:
625   27-45.

626   Bailey, R.T., T.K. Gates, and M. Ahmadi (2014), Simulating reactive transport of selenium
627   coupled with nitrogen in a regional-scale irrigated groundwater system. J. Hydrol. 515: 29-46.

628   Bailey, R.T. and M. Ahmadi (2014), Spatial and temporal variability of in-stream water quality
629   parameter influence on dissolved oxygen and nitrate within a regional stream network.
630   Ecological Modelling 277, 87-96. doi: 10.1016/j.ecolmodel.2014.01.015.

631   Bailey, R.T., Gates, T.K., and E.C. Romero (2015), Assessing the effectiveness of land and
632   water management practices on nonpoint source nitrate levels in an alluvial stream-aquifer
633   system. J. Cont. Hydrology 179, 102-115.

634   Birkinshaw, S.J., and J. Ewen (2000), Nitrogen transformation component for SHETRAN
635   catchment nitrate transport modelling. J. Hydrol. 230: 1-17.

636   Botter, G., Settin, T., Marani, M., and A. Rinaldo (2006), A stochastic model of nitrate transport
637   and cycling at basin scale. Water Res. Research 42, doi: 10.1029/2005WR004599.

638   Cacuci, D. G. (2003), Sensitivity and Uncertainty Analysis, Volume I: Theory, CRC Press, Boca
639   Raton, Florida.

640   Campolongo, F. and A. Saltelli (1997), Sensitivity analysis of an environmental model: an
641   application of different analysis methods. Reliability Engineering & System Safety 57(1), 49–69,
642   doi: 10.1016/S0951-8320(97)00021-5.

643 Campolongo, F. and R. Braddock, R. (1999), Sensitivity analysis of the IMAGE Greenhouse

644 model. Environmental Modelling & Software 14(4), 275–282, doi: 10.1016/S1364-

645 8152(98)00079-6.

646 Campolongo, F., J. Cariboni, and A. Saltelli (2007), An effective screening design for sensitivity

647 analysis of large models, Environmental Modelling & Software 22(10), 1509–1518,

648 doi:10.1016/j.envsoft.2006.10.004.

649 Colorado Department of Public Health and Environment (CDPHE). 2012. "Regulation No. 31:

650 The Basic Standards and Methodologies for Surface Water." Denver, Colorado.

651 Chaplot, V., A. Saleh, D.B. Jaynes, and J. Arnold (2004), Predicting water, sediment and NO_3-N

652 loads under scenarios of land-use and management practices in a flat watershed., Water, Air, and

653 Soil Pollution 154: 271-293.

654 Conan, E., F. Bouraoui, N. Turpin, G. de Marsily, and G. Bidoglio (2003), Modeling flow and

655 nitrate fate at catchment scale in Brittany (France). J. Environ. Qual., 32: 2026-2032.

656 Cox, B.A., and P.G. Whitehead (2005), Parameter sensitivity and predictive uncertainty in a new

657 water quality model, Q^2. J. Environ. Engr. 131, 147-157.

658 Cukier, R., Fortuin, C.M., Schuler, K.E., Petschek, A.G., and J.H. Schaibly (1973), Study of the

659 sensitivity of coupled reaction systems to uncertainties in rate coefficients. i theory. J. Chem.

660 Physics 59, 3873-3878.

661 Deflandre, A., R.J. Williams, F.J. Elorza, J. Mira, and D.B. Doorman (2006), Analysis of the

662 QUESTOR water quality model using a Fourier amplitude sensitivity test (FAST) for two UK

663 rivers. Science of the Total Environ. 360, 290-304.

664 Ehteshami, M., A.S. Langeroudi, and S. Tavassoli (2013), Simulation of nitrate contamination in

665 groundwater caused by livestock industry (cast study: Rey). J. Environ. Protection 4, 91-97.

666   Fan, A.M., and V.E. Steinberg (1996), Health implications of nitrate and nitrite in drinking

667   water: an update on methemoglobinemia occurrence and reproductive and developmental

668   toxicity. Regulatory Toxicology and Pharmacology 23, 35-43.

669   Frind, E.O., W.H.M. Duynisveld, O. Strebel, J. Boettcher (1990), Modeling of multicomponent

670   transport with microbial transformation in groundwater: the Fuhrberg case. Water Resour. Res.

671   26 (8), 1707–1719.

672   Gates, T.K., B.M. Cody, J.P. Donnelly, A.W. Herting, R.T. Bailey, and J. Mueller-Price (2009),

673   Assessing Selenium contamination in the irrigated stream-aquifer system of the Arkansas River,

674   Colorado. J. Environ. Qual., 38: 2344-2356.

675   Hall J.W., Tarantola S., Bates P.D., and M.S. Horritt (2005), Distributed sensitivity analysis of

676   flood inundation model calibration. J. Hydraul. Eng. 131:117 – 26.

677   Hall, J. W., S. A. Boyce, Y. Wang, R. J. Dawson, S. Tarantola, and A. Saltelli (2009), Sensitivity

678   analysis for hydraulic models, J. Hydraul. Eng., 135(11), 959, doi:10.1061/(ASCE)HY.1943-

679   7900.0000098.

680   Hartmann, A., Weiler, M., Wagener, T., Lange, J., Kralik, M., Humer, F., Mizyed, N., Rimmer,

681   A., Barberá, J. A., Andreo, B., Butscher, C. and P. Huggenberger (2013), Process-based karst

682   modelling to relate hydrodynamic and hydrochemical characteristics to system properties.

683   Hydrol. Earth Syst. Sci., 17(8), 3305–3321, doi:10.5194/hess-17-3305-2013.

684   Hefting, M.M., and J.J.M. de Klein (1998), Nitrogen removal in buffer strips along a lowland

685   stream in the Netherlands: a pilot study. Environ. Pollut., 102, 521–526.

686   Holloway, J. M., and R. A. Dahlgren. (2002). Nitrogen in rock: Occurrences and

687   biogeochemical implications. Global Biogeochem. Cycles, 16(4), 65-1 – 65-17.

688   Iman, R.L. and W.J. Conover (1987), A measure of top-down correlation. Technometrics

689   293, 351-357.

690   Johnsson, H., L. Bergström, P. Jansson, and K. Paustian (1987), Simulated nitrogen dynamics

691   and losses in a layered agricultural soil. Agric. Ecosyst. Environ. 18: 333-356.

692   Jørgensen, C.J., O.S. Jacobsen, B. Elberling, and J. Aamand (2009), Microbial oxidation of

693   pyrite coupled to nitrate reduction in anoxic groundwater sediment. Environ. Sci. Technol. 43,

694   4851-4857.

695   Kelleher, C., Wagener, T., McGlynn, B., Ward, A. S., Gooseff, M. N. and R. A. Payn (2013),

696   Identifiability of transient storage model parameters along a mountain stream, Water Resour.

697   Res., doi:10.1002/wrcr.20413.

698   Korom, S.F. (1992), Natural denitrification in the saturation zone: a review. Water Resour. Res.

699   28 (6), 1657–1668.

700   Lee, M., G. Park, M. Park, J. Park, J. Lee, and S. Kim (2010), Evaluation of non-point source

701   pollution reduction by applying best management practices using a SWAT model and QuickBird

702   high resolution satellite imagery. J. Environmental Sciences 22(6): 826-833.

703   Liu, D., and Z. Zou (2012), Sensitivity analysis of parameters in water quality models and water

704   environment management. J. Environmental Protection 3, 863-870.

705   Ma, L., M. J. Shaffer, J. K. Boyd, R. Waskom, L. R. Ahuja, K. W. Rojas, and C. Xu (1998),

706   Manure Management in an Irrigated Silage Corn Field: Experiment and Modeling. Soil Sci. Soc.

707   Am. J. 62:1006-1017.

708   McNab Jr., W.W., and B.P. Dooher (1998), Uncertainty analysis of fuel hydrocarbon

709   biodegradation signatures in groundwater by probabilistic modeling. Ground Water 36 (4), 69–

710   698.

711   Molénat, J. and C. Gascuel-Odoux (2002), Modelling flow and nitrate transport in groundwater

712   for the prediction of water travel times and of consequences of land use evolution on water

713   quality. Hydrological Processes 16, 479-492.

714   Montross, G. G., B. L. McGlynn, S. N. Montross, and K. K. Gardner (2013), Nitrogen
715   production from geochemical weathering of rocks in southwest Montana, USA. J. Geophys.
716   Res.: Biosci., 118, 1068-1078.

717   Morris, M., 1991. Factorial sampling plans for preliminary computational experiments.
718   Technometrics 33(2), 161–174.

719   Morway, E. D., and T.K. Gates (2012), Regional assessment of soil water salinity across an
720   intensively irrigated river valley. J. Irrig. Drain. Engrg, 138(5): 393-405.

721   Morway, E. D., T.K. Gates, and R.G. Niswonger (2013), Appraising options to enhance shallow
722   groundwater table and flow conditions over regional scales in an irrigated alluvial aquifer
723   system. J. Hydrol., 495: 216-237.

724   Niswonger, R.G., D.E. Prudic, and R.S. Regan (2006), Documentation of the unsaturated-zone
725   flow (UZF1) package for modeling unsaturated flow between the land surface and the water
726   table with MODFLOW-2005, U.S. Geological Survey Techniques and Methods 6-A19.

727   Niswonger, R.G., S. Panday, and I. Motomu (2011), MODFLOW-NWT, A Newton formulation
728   for MODFLOW-2005: U.S. Geological Survey Techniques and Methods 6–A37: 44 p.

729   Ocampo, C.J., M. Sivapalan, and C.E. Oldham (2006), Field exploration of coupled hydrological
730   and biogeochemical catchment responses and a unifying perceptual model. Adv. Water Resour.,
731   29, 161-180.

732   Oyarzun, R., J. Arumí, L. Salgado, and M. Mariño (2007), Sensitivity analysis and field testing
733   of the RISK-N model in the Central Valley of Chile. Agricul. Water Management 87, 251-260.

734   Parkin, T.B. and J.A. Robinson (1989), Stochastic models of soil denitrification. Appl. Environ.
735   Micro. 55 (1), 72–77.

736   Reusser, D.E., W. Buytaert, and E. Zehe (2011), Temporal dynamics of model parameters
737   sensitivity for computationally expensive models with the Fourier amplitude sensitivity test.
738   Water Resources Research 47, W07551,doi:10.1029/2010WR009947.

739   Rong, Y., and W. Xuefeng (2011), Effects of nitrogen fertilizer and irrigation rate on nitrate

740   present in the profile of a sandy farmland in Northwest China. Procedia Environ. Sci. 11: 726-

741   732.

742   Sahu, M., and R.R. Gu (2009), Modeling the effects of riparian buffer zone and contour strips on

743   stream water quality, Ecol. Engr. 35: 1167-1177.

744   Saltelli, A., M. Ratto, T. Andres, F. Campolongo, J. Cariboni, D. Gatelli, M. Saisana, and S.

745   Tarantola (2008), Global Sensitivity Analysis. The Primer, John Wiley and Sons. West Sussex,

746   England.

747   Schilling, K.E., Tomer, M.D., Zhang, Y.-K., Weisbrod, T., and P. Jacobson (2007),

748   Hydrogeologic controls on nitrate transport in a small agricultural catchment, Iowa. J. Geoph.

749   Reseasrch 112, doi:10.1029/2007JG000405.

750   Scott, G. R. (1968), Geologic and structure contour map of the La Junta quadrangle, Colorado

751   and Kansas, edited by U. S. G. Survey, Reston, Virginia.

752   Sharps, J. A. (1976), Geologic map of the Lamar quadrangle, Colorado and Kansas, edited by U.

753   S. G. Survey, Reston, Virginia.

754   Sincock, A.M., H.S. Wheater, and P.G. Whitehead (2003), Calibration and sensitivity analysis of

755   a river water quality model under unsteady flow conditions. J. Hydrology 227, 214-229.

756   Sobol', I.M. (1993), Sensitivity analysis for non-linear mathematical models. Mathematical

757   Modelling and Computational Experiment 1, 407-414.

758   Spalding, R.F., and M.E. Exner (1993), Occurrence of nitrate in groundwater: A review. J.

759   Environ. Qual.22, 392-402.

760   Spruill, T.B. (2000), Statistical evaluation of effects of riparian buffers on nitrate and ground

761   water quality, J. Environ. Qual. 29: 1523-1538.

762   Sun, X., L. Newham, B. Croke, and J. Norton (2012), Three complementary methods for

763   sensitivity analysis of a water quality model. Environmental Modelling & Software 37, 19–29,

764   doi: 10.1016/j.envsoft.2012.04.010.

765   Vaché, K.B., J.M. Eilers, and M.V. Santelmann (2002), Water quality modeling of alternative

766   agricultural scenarios in the U.S. Corn Belt, J. Amer. Water Resour. Assoc. 38(3): 773-787.

767   White, K. L., and I. Chaubey (2005), Sensitivity analysis, calibration, and validations for a

768   multisite and multivariable SWAT model, J. Am. Water Resour. Association, 41(5), 1077–1089,

769   doi:10.1111/j.1752-1688.2005.tb03786.x.

770   Wriedt, G., and M. Rode (2006), Modelling nitrate transport and turnover in a lowland

771   catchment system. J. Hydrol., 328, 157-176.

772   Wu, W.-M., J. Carley, S.J. Green, J. Luo, S.D. Kelly, J.V. Nostrand, K. Lower, T. Mehlhorn, S.

773   Carroll, B. Boonchayanant, F.E. Löfller, D. Watson, K.M. Kemner, J. Zhou, P.K. Kitanidis, J.E.

774   Kostka, P.M. Jardine, and C.S. Criddle (2010), Effects of nitrate on the stability of uranium in a

775   bioreduced region of the subsurface. Environ. Sci. Techno,. 44, 5104-5111.

776   Zielinski, R. A., S. Asher-Bolinder, A. L. Meier, C. A. Johnson, and B. J. Szabo. (1997). Natural

777   or fertilizer-derived uranium in irrigation drainage: a case study in southeastern Colorado, USA.

778   Appl. Geochem., 12, 9 – 21.

779

780

781

782

783

784 Table 1. Baseline agricultural management and crop parameter values for the model simulations.

Crop Type	Planting Day	Harvest Day	Plow Day	P_{St}	$d_{rt,max}$	CN_{RT}	F_{NH_4}	N_{up}
Units	-	-	-	kg ha^{-1}	m	-	kg ha^{-1}	kg ha^{-1}
Alfalfa	30-Apr	30-Sep	20-Oct	561.6	1.83	25	22.4	22.4
Bean	20-May	30-Sep	20-Oct	561.6	0.91	25	140	84.2
Corn	1-May	25-Oct	14-Nov	5616	1.22	70	252	224.6
Melon	15-May	10-Aug	30-Aug	561.6	1.22	25	112	112.3
Onion	20-Mar	15-Sep	5-Oct	561.6	0.46	25	140	78.6
Pasture	30-Aug	30-Sep	20-Oct	0	0.91	70	140	112.3
Pumpkin	1-Jun	30-Sep	20-Oct	561.6	0.91	25	140	84.2
Sorghum	20-May	15-Oct	4-Nov	1684.8	0.91	70	112	112.3
Spring Grain	1-Apr	15-Jul	4-Aug	1684.8	0.91	70	112	112.3
Squash	20-May	25-Jul	14-Aug	561.6	0.91	25	140	84.2
Sunflower	1-Jun	10-Oct	30-Oct	561.6	0.91	25	140	84.2
Vegetable	25-Apr	30-Aug	19-Sep	561.6	0.91	25	140	84.2
Winter Wheat	30-Sep	5-Jul	25-Jul	1684.8	0.91	70	112	112.3

785 d_{pw} (depth of plowing) is 1.0 m for all crops except beans (0.8 m)
786 P_{Rt} (seasonal mass of root mass) is 500 kg ha^{-1} for all crop types
787 CN_{ST} (carbon:nitrogen ratio in stover mass) is 50 for all crop types

788

789 Table 2. Parameters and values for chemical reactions involving organic matter decomposition, dissolved oxygen,

790 and nitrogen species for the baseline simulation model.

Org. Matter Decomp.			Dissolved Oxygen			Nitrogen		
Param.	Value	Unit	Param.	Value	Unit	Param.	Value	Unit
λ_L	0.25	d^{-1}	$\lambda_{O_2}^{het}$	2.0	d^{-1}	$H_{C/N}$	12.0	-
λ_H	0.003	d^{-1}	$\lambda_{O_2}^{auto}$ *	0.58	d^{-1}	$B_{C/N}$	8.0	-
f_e	0.5	-	K_{O_2}	1.0	g m$_f^{-3}$	I_{O_2}	1.0	g m$_f^{-3}$
f_h	0.2	-				λ_{nit} *	0.98	d^{-1}
K_{CO_2}	0.75	g m$_f^{-3}$				λ_{vol}	0.1	d^{-1}
						$\lambda_{NO_3}^{het}$	0.1	d^{-1}
						$\lambda_{NO_3}^{auto}$ *	0.22	d^{-1}
						K_{NO_3}	10.0	g m$_f^{-3}$
						K_{d,NH_4}	3.5	-

791 * Indicates mean value, with specific values assigned to each command area according to the values reported in Bailey et al. (2014).

792

793

794

795

796

797

798

799

800 Table 3. Sensitivity index (μ*) for each of the model input factors investigated, indicating the degree of parameter

801 influence on C_{NO_3} in the shallow saturated zone of the aquifer (in layer 4 of the grid) for the grid cells associated with

802 each crop type and command area, with the values of the top three influential parameters for each crop type and

803 command area bolded.

	N Fert. Loading	N uptake	Litter decomp.	Humus decomp.	O₂ reduction	Nitrif.	Het. Denitrif.	Auto. Denitrif.	NO₃ canal conc.
	F_{NH_4}	N_{up}	λ_L	λ_H	$\lambda_{O_2}^{auto}$	λ_{nit}	$\lambda_{NO_3}^{het}$	$\lambda_{NO_3}^{auto}$	$Canal_{NO_3}$
Crop									
Alfalfa	**0.46**	**0.56**	0.03	0.09	0.00	0.06	**0.23**	0.04	0.11
Bean	**0.70**	**0.43**	0.04	0.09	0.00	0.03	**0.34**	0.00	0.06
Corn	**0.94**	**0.72**	0.04	0.10	0.00	0.03	**0.30**	0.03	0.09
Melon	**5.46**	**3.02**	0.10	0.15	0.00	0.23	**0.92**	0.00	0.47
Onion	**1.21**	**0.99**	0.02	0.14	0.00	0.03	0.19	0.01	**0.45**
Pasture	**0.66**	**0.63**	0.03	0.12	0.01	0.04	**0.32**	0.07	0.14
Sorghum	**0.84**	**0.81**	0.03	0.12	0.00	0.08	**0.28**	0.04	0.13
Spring Grain	**0.79**	**0.70**	0.04	0.13	0.00	0.02	**0.32**	0.02	0.06
Command Area									
Catlin	**0.12**	**0.26**	0.00	0.03	0.01	**0.16**	0.04	0.01	0.11
Fort Lyon	**0.92**	**0.81**	0.05	0.17	0.00	0.04	**0.42**	0.08	0.12
Highline	**0.69**	**0.51**	0.03	0.06	0.00	0.02	0.23	0.01	**0.26**
Holbrook	**0.28**	**0.29**	0.02	0.03	0.00	0.01	0.08	**0.11**	0.10
Otero	**1.21**	**1.16**	0.05	0.14	0.00	0.04	0.49	0.04	**0.59**
RF Ditch	0.14	**0.15**	0.01	0.03	0.02	0.01	0.14	**0.20**	**0.51**

804

805

806

807

808

809

810

811

812

813

814

815

816

817

818 Table 4. Sensitivity index (μ^*) for each of the model input factors investigated, indicating the degree of parameter

819 influence on NO$_3$ mass leaching from the shallow soil zone for the grid cells associated with each crop type and

820 command area, , with the values of the top three influential parameters for each crop type and command area bolded.

	N Fert. Loading	N uptake	Litter decomp.	Humus decomp.	O$_2$ reduction	Nitrif.	Het. Denitrif.	Auto. Denitrif.	NO$_3$ canal conc.
	F_{NH_4}	N_{up}	λ_L	λ_H	$\lambda_{O_2}^{auto}$	λ_{nit}	$\lambda_{NO_3}^{het}$	$\lambda_{NO_3}^{auto}$	$Canal_{NO_3}$
Crop Type									
Alfalfa	**396**	**614**	19	73	0.8	39	**176**	13	108
Bean	**43**	**26**	2.7	7.6	0.0	2.3	**22**	0.0	3.6
Corn	**486**	**367**	26	51	0.2	15	**172**	1.0	41
Melon	**7.0**	**4.5**	0.2	0.2	0.0	0.2	**1.9**	0.0	0.6
Onion	**9.7**	**7.2**	0.2	0.4	0.0	0.4	1.1	0.0	**1.6**
Pasture	**431**	**382**	16	76	0.4	9.0	**162**	12	49
Sorghum	**271**	**221**	11	29	0.1	11	**94**	2.1	26
Spring Grain	**213**	**179**	11	31	0.2	2.9	**82**	1.3	14
Command Area									
Catlin	**35**	**63**	0.9	5.3	0.1	**38**	7.5	0.3	9.2
Fort Lyon	**852**	777	35	140	1.0	33	**335**	13	70
Highline	**125**	**103**	4.2	12	0.0	2.7	**41**	0.1	37
Holbrook	**70**	**71**	3.6	5.7	0.1	2.6	**21**	3.6	10
Otero	**196**	**176**	8.4	21	0.0	4.7	**85**	2.0	62
RF Ditch	**3.6**	**3.9**	0.1	1.2	0.2	0.5	1.9	3.3	**30**

821
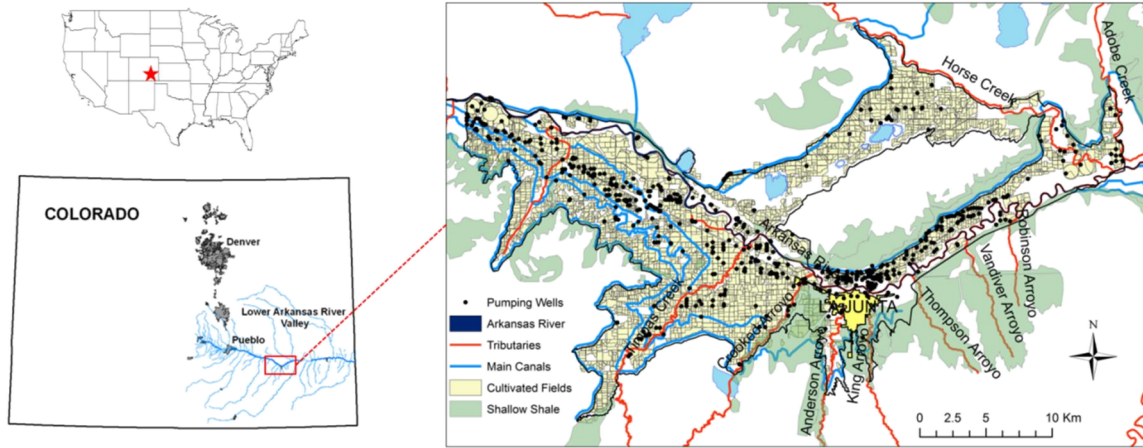
822

823

824

825

826

827

828

829

830

Figure 1. Location and hydrologic features of the study region in the Lower Arkansas River Valley in southeastern Colorado, showing the Arkansas River and tributaries (red), cultivated fields (yellow), irrigation canals (light blue), groundwater pumping wells (black dots), and the extent of near-surface shale (within 2 m of the ground surface) (green).
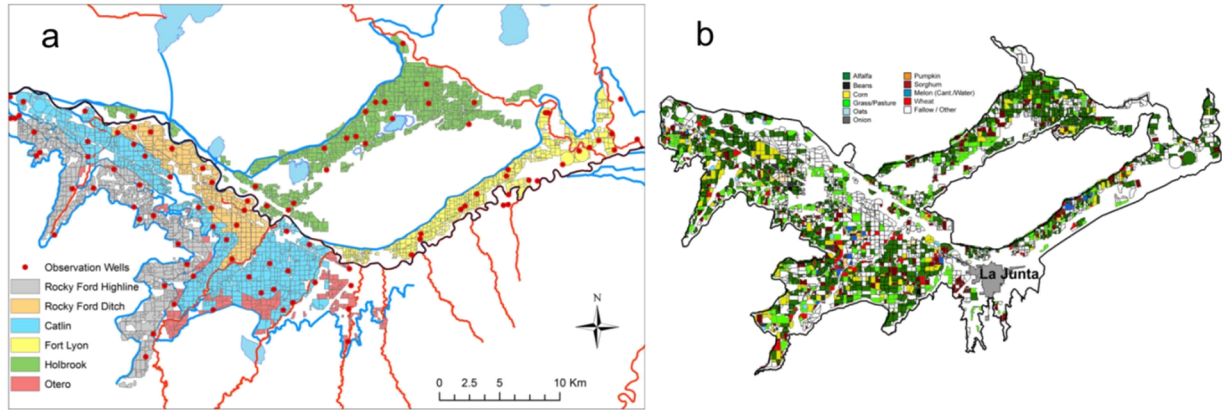
Figure 2. Features of the cultivation and data collection of the study region, including (a) canal command areas and location of groundwater observation wells, with a command area defined as the collection of fields receiving irrigation water from the same canal, and (b) the spatial distribution of crop cultivation during the 2006 growing season.
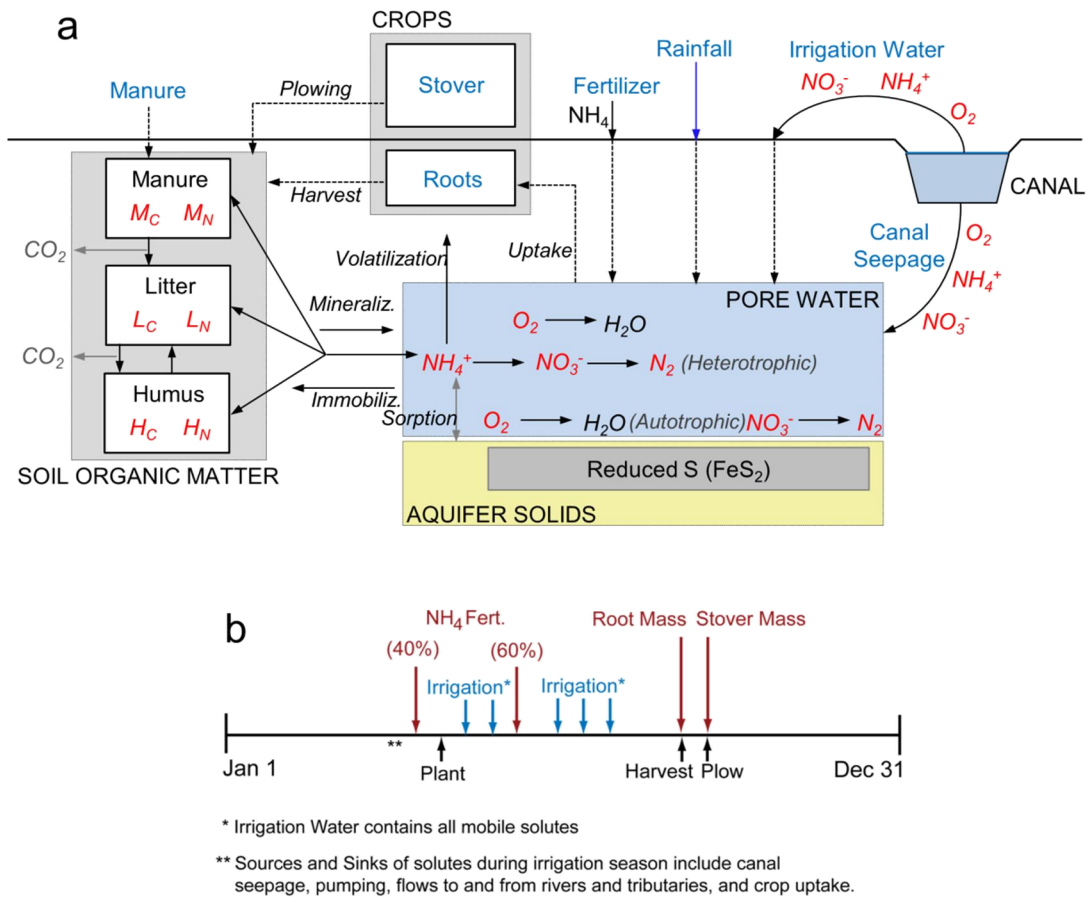
Figure 3. Depiction of the main processes simulated by the N reaction module of the UZF-RT3D model, with (a) conceptual model of the fate and transport of O_2 and N species in an irrigated soil-aquifer system wherein fertilizer, irrigation, and canal seepage bring solute mass into the subsurface environment, and (b) the annual cultivation schedule used in the N reaction module, including timing of planting, fertilizer loading, irrigation application, harvest, and plowing. NH_4 fertilizer has a split loading, with 40% of the loading occurring 2 weeks before planting, and the remainder applied 6 weeks after planting.

874
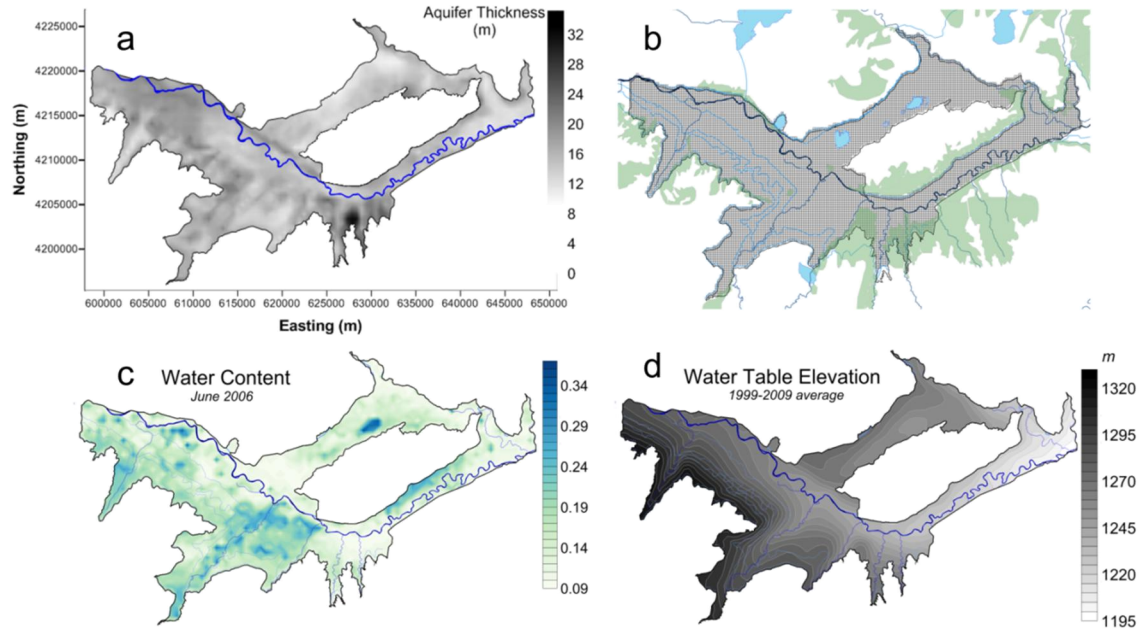
875   Figure 4. (a) The spatial distribution of aquifer thickness (m) of the alluvium in the study region, (b) the finite-

876   difference grid used in the calibrated and tested MODFLOW-UZF1 groundwater flow model, using 250 m by 250 m

877   grid cells, (c) spatial distribution of soil water content simulated by the MODFLOW-UZF1 model, for June 2006,

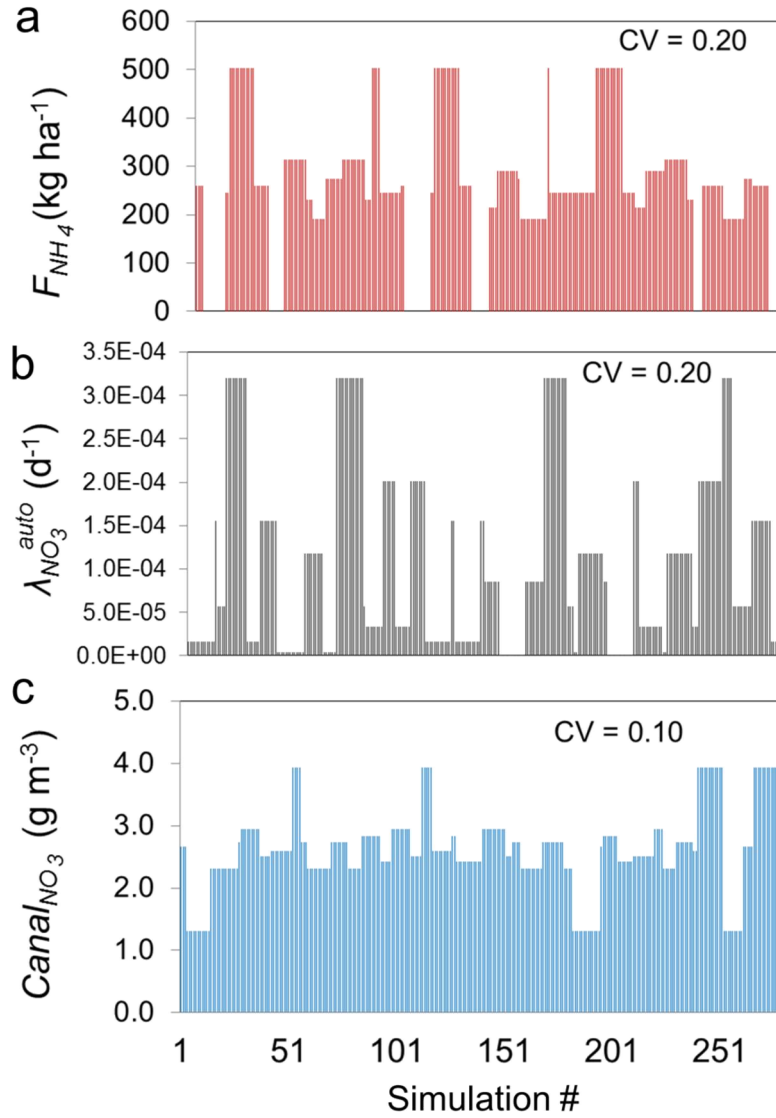878   and (d) average-simulated water table elevation for the 1999-2009 time period.

879

880

881

882
883
884
885
886
887
888
889
890

891

Figure 5. Values of (a) fertilizer loading F_{NH_4} (kg/ha) for corn, and (b) first-order rate constant of autotrophic

denitrification $\lambda^{auto}_{NO_3}$ (1/day) and (c) nitrate concentration of canal water $Canal_{NO_3}$ (mg/L) for the Rocky Ford Highline

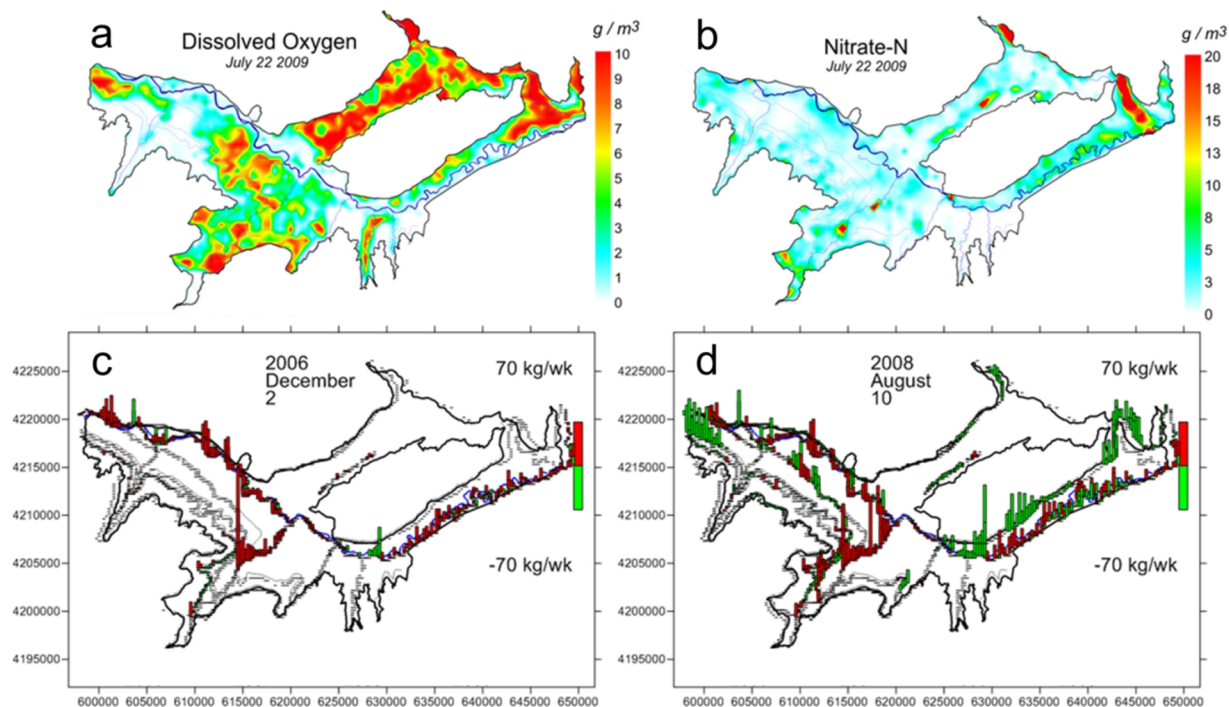canal command area, for each of the 280 simulations in the revised Morris SA scheme.

899

Figure 6. Summary of typical UZF-RT3D model results for the study region, showing spatial distribution of (a) C_{O_2}

and (b) C_{NO_3} in shallow groundwater, and spatial distribution of mass loadings of nitrate to the Arkansas River

system (main stem and tributaries) for (c) December 2 2006, and (d) August 10 2008, showing the contrast between

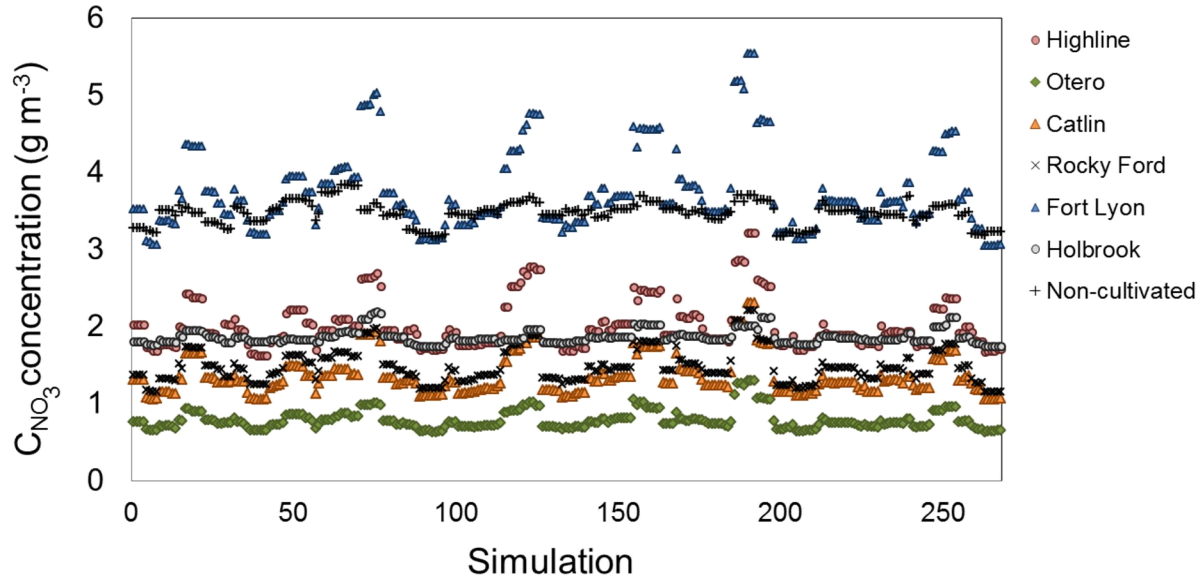the winter and summer seasons.

904

905

906

907

908

909 Figure 7. Spatio-temporal average value of C_{NO_3} in groundwater during the 2006-2009 simulation period for each

910 canal command area for each of the 280 UZF-RT3D model simulations. The spatio-temporal average for the non-

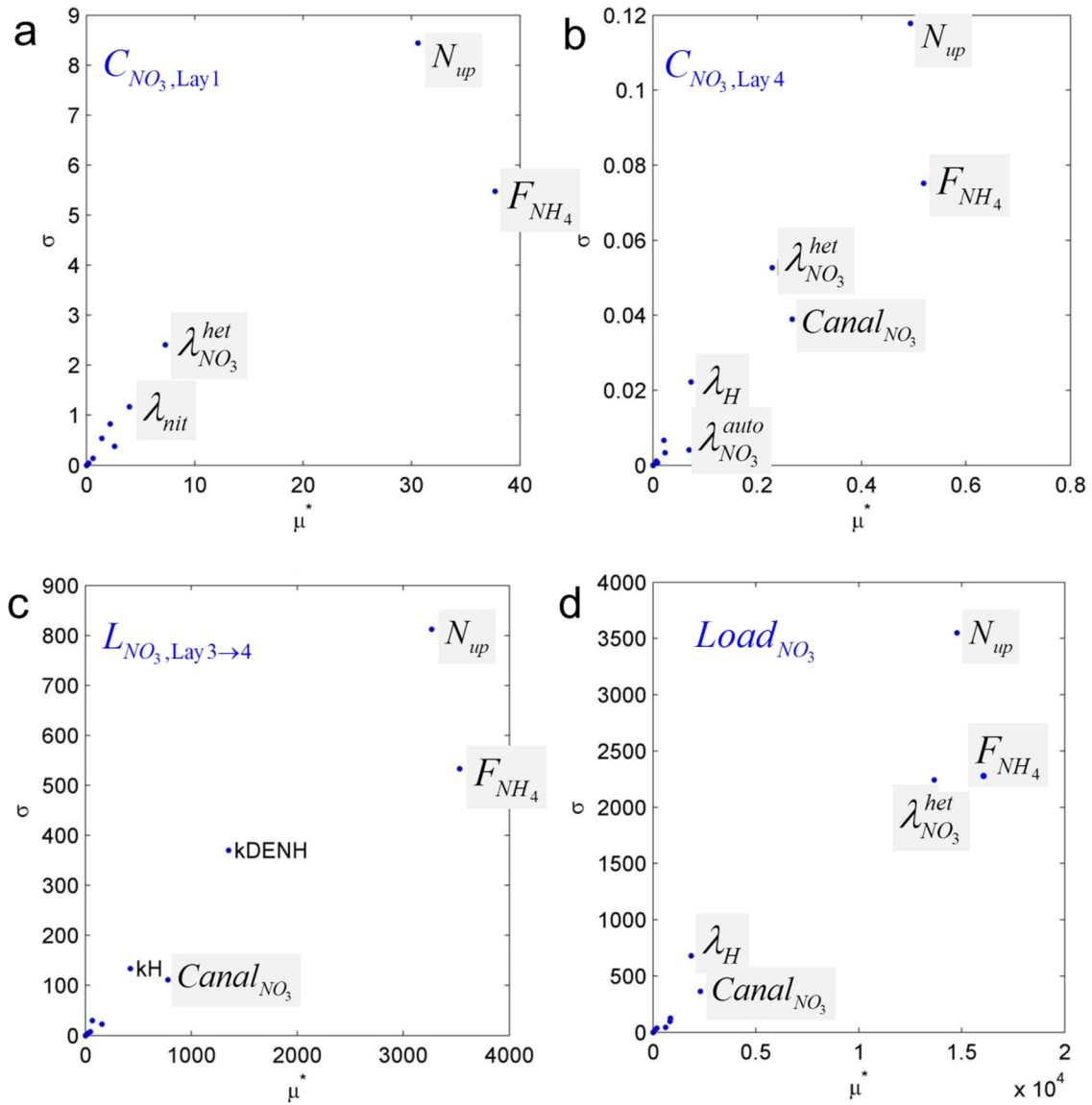911 cultivated areas also is shown (small black crosses).

912

913

914

915

916

917

918

919

920

921

922

923

924

925

Figure 8. Global sensitivity plots (σ vs. μ^*) showing influence of the 9 targeted model input factors on (a) C_{NO_3} in Layer 1 of the model (top 0.5 m of the root zone), (b) C_{NO_3} in Layer 4 of the model (shallow saturated zone of the aquifer), (c) NO₃ mass leaching from Layer 3 to Layer 4 (unsaturated zone to saturated zone), and (d) total mass loading of NO₃ from the aquifer to the Arkansas River.

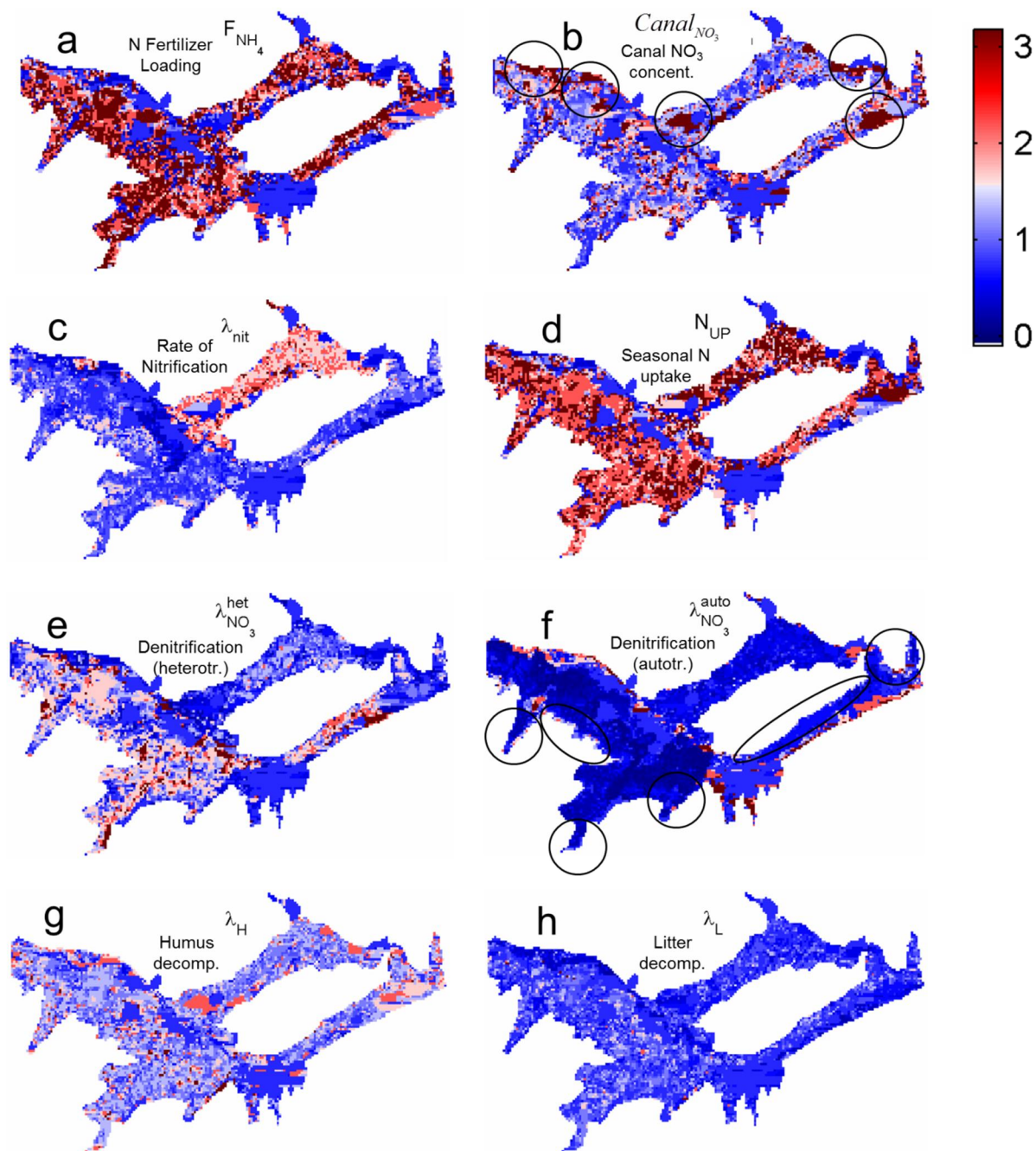Figure 9. Cell-by-cell (250 m by 250 m) plots of Savage scores for (a) F_{NH_4}, (b) $Canal_{NO_3}$, (c) λ_{nit},(d) N_{up}, (e) $\lambda_{NO_3}^{het}$, (f) $\lambda_{NO_3}^{auto}$, (g) λ_H, and (h) λ_L indicating the ranking of influence of that parameter on C_{NO_3} in groundwater for each of the 7,776 cells in the study region.

942

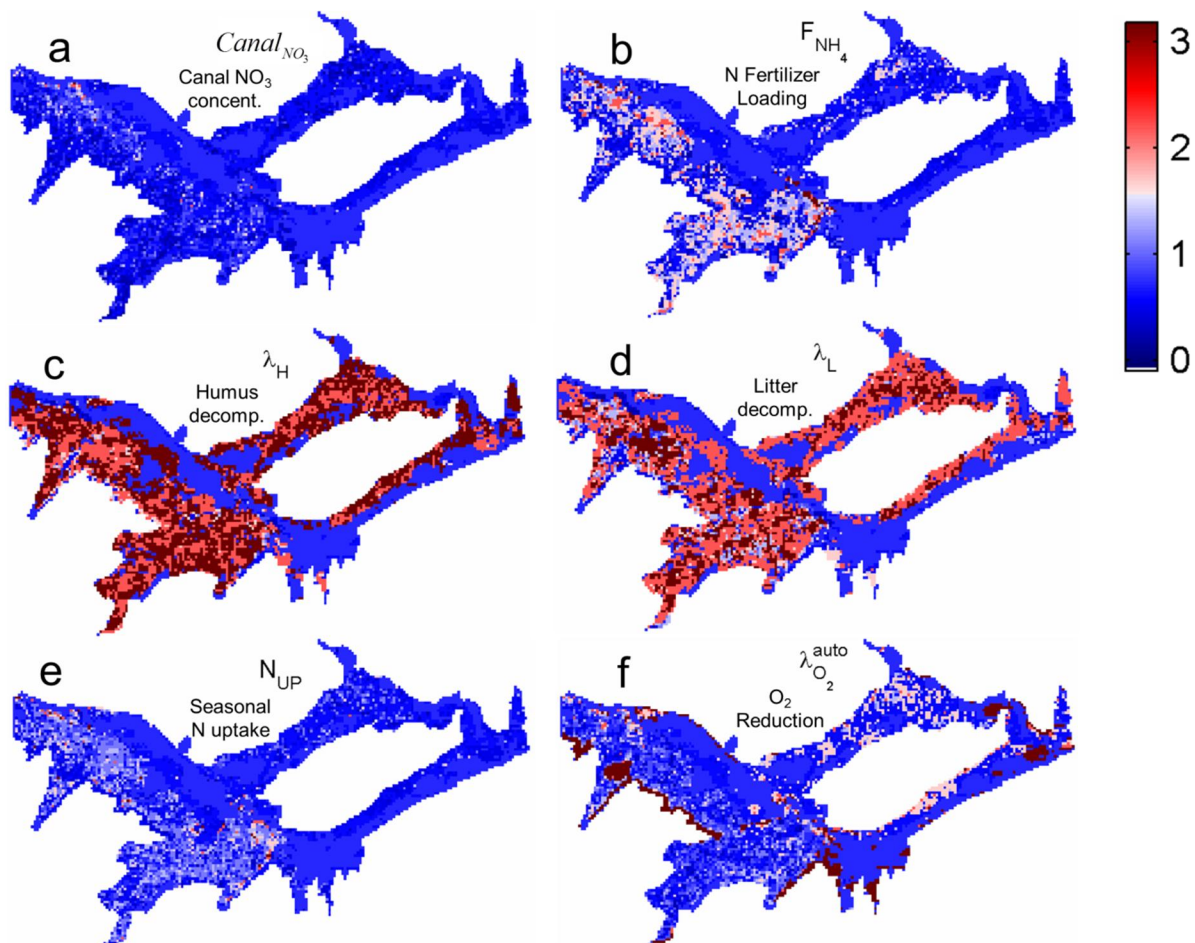Figure 10. Cell-by-cell (250 m by 250 m) plots of Savage scores for (a) $Canal_{NO_3}$, (b) F_{NH_4}, (c) λ_H, (d) λ_L, (e) N_{up}, and (f) $\lambda_{O_2}^{auto}$, indicating the ranking of influence of that parameter on C_{O_2} in groundwater for each of the 7,776 cells in the study region.

946

947

948

949

950